

SIMPLE AND CONTROLLABLE UNIFORM DISCRETE DIFFUSION LANGUAGE MODELS

Anonymous authors

Paper under double-blind review

ABSTRACT

Diffusion models for continuous data gained widespread adoption owing to their high quality generation and control mechanisms. However, controllable diffusion on discrete data faces challenges: continuous diffusion guidance methods are not applicable and recent discrete diffusion models are not well-suited to control or exhibit a quality gap. Here, we provide a straightforward derivation of classifier-free and classifier-based guidance for discrete diffusion, as well as a new class of diffusion models that leverage uniform noise and thus can continuously edit their outputs. We improve the quality of these models with a novel continuous-time variational lower bound that yields state-of-the-art performance, in settings with small vocabularies. Empirically, we demonstrate the effectiveness of our guidance mechanisms relative to autoregressive and diffusion baselines, especially in conjunction with uniform noise diffusion, on several discrete data domains, including genomic sequences, small molecule design, and discretized image generation.

1 INTRODUCTION

Diffusion models (Sohl-Dickstein et al., 2015; Ho et al., 2020) gained widespread adoption in image generation and signal processing in part due to their high controllability using mechanisms such as classifier-based (Dhariwal & Nichol, 2021a) and classifier-free (Nichol et al., 2021; Ho & Salimans, 2022) guidance. Tasks where guidance plays a key role include MRI denoising (Song & Ermon, 2019), 3D reconstruction (Poole et al., 2022; Gao et al., 2024), and conditional generation (Saharia et al., 2022; Gokaslan et al., 2024).

However, applying controllable diffusion-based generation to tasks where the data is discrete (e.g., molecule design or text generation) presents challenges. First, standard diffusion models and their guidance mechanisms are not directly applicable, since they require taking gradients with respect to the data, and these are not defined in discrete settings. Second, popular discrete extensions of diffusion (Lou et al., 2023; Sahoo et al., 2024a) cannot perform multiple editing passes on generated tokens, hence are not ideal for controllable generation. Third, the performance of discrete diffusion models (measured by perplexity) lags behind autoregressive (AR) models, especially for classes of diffusion that are amenable to control, such as uniform noise (Austin et al., 2021; Lou et al., 2023).

Here, we propose discrete diffusion models and guidance mechanisms that are effective at controllable generation and that address the above challenges. First, we provide straightforward and easy to implement adaptations of classifier-based and classifier-free guidance for discrete diffusion models. Second, we introduce uniform noise diffusion language models (UDLM), which undo random token perturbations and are particularly amenable to guidance, since they can continuously edit discrete data (Austin et al., 2021). Third, we address performance issues that plagued previous iterations of uniform noise discrete diffusion, namely, we introduce a continuous time version of the evidence lower bound which tightens the variational gap (Kingma et al., 2021; Sahoo et al., 2024a).

We demonstrate the effectiveness of guidance with discrete diffusion models relative to AR models on several domains: genomics, molecular generation, and discretized images. Our guidance results indicate that classifier-free guidance is more useful when paired with diffusion models compared to AR and that our proposal for classifier-based guidance is the best classifier-based method for discrete guidance, especially when combined with UDLM. Our language modeling experiments reveal that contrary to a widely-held belief (Austin et al., 2021; Lou et al., 2023), uniform noise diffusion can

attain state-of-the-art performance on small vocabulary datasets (e.g., molecules, DNA) and that UDLM attains a new state-of-the-art in perplexity among uniform noise diffusion models.

In summary, our contributions are as follows:

- We provide simple and effective discrete classifier-based and classifier-free guidance.
- We introduce UDLM, a class of discrete diffusion models particularly amenable to guidance, and we derive a tightened ELBO that significantly improves their performance.
- Across three domains, we demonstrate that discrete guidance yields better controllable generation compared to strong AR baselines and previous diffusion guidance methods.

2 BACKGROUND

Notation Let \mathcal{V} be the space of all one-hot tokens over some vocabulary consisting of N unique characters: $\mathcal{V} = \{\mathbf{z} \in \{0, 1\}^N : \sum_i \mathbf{z}_i = 1\} \subset \Delta^N$, where Δ^N represents the simplex over N categories. Let $\mathbf{1}$ be a N -dimensional column vector of all ones, and denote the Hadamard product between two vectors as \odot . We define $\mathbf{z}^{(1:L)}$ as a sequence of L tokens, where $\mathbf{z}^{(\ell)} \in \mathcal{V}$, for all tokens $\ell \in 1, \dots, L$, and use \mathcal{V}^L to denote the set of all such sequences. Finally, let $\text{Cat}(\cdot; p)$ denote the categorical distribution with probability vector $p \in \Delta^N$.

2.1 DISCRETE DIFFUSION MODELS

Diffusion models are a class of generative models defined by a denoising network p_θ that is trained to remove noise from latent variables \mathbf{z}_t . These latents are generated by a fixed corruption process q that, starting from clean data \mathbf{x}_0 drawn from the data distribution $q(\mathbf{x}_0)$, increasingly adds more noise to \mathbf{z}_t , as t increases (Sohl-Dickstein et al., 2015; Song & Ermon, 2019; Ho et al., 2020).

In discrete denoising diffusion probabilistic models (D3PM; Austin et al. (2021)), the noising process is defined in terms of a transition matrix $Q_{t|s}$ whose (i, j) th entry is the probability of transitioning from the i -th state at time s to the j -th state at time t . This induces a Markov corruption process where we have $q(\mathbf{z}_t | \mathbf{z}_s) = \text{Cat}(\mathbf{z}_t; Q_{t|s}\mathbf{z}_s)$. Sahoo et al. (2024a) build off this framework to introduce specialized algorithms that are both simpler and more effective than the general D3PM framework. They focus on a specific class of forward processes from D3PM that can be defined as interpolations between clean data and a noisy prior $\boldsymbol{\pi}$, and we adopt their notation below:

$$q(\mathbf{z}_t | \mathbf{x}_0) = \text{Cat}(\mathbf{z}_t; \alpha_t \mathbf{x}_0 + (1 - \alpha_t) \boldsymbol{\pi}), \quad (1)$$

where $\alpha_t = \alpha(t)$ is a noise schedule monotonically decreasing in t . Defining $\alpha_{t|s} = \alpha_t / \alpha_s$, this class of processes admit the following posteriors

$$q(\mathbf{z}_s | \mathbf{z}_t, \mathbf{x}_0) = \text{Cat} \left(\mathbf{z}_s; \frac{[\alpha_{t|s} \mathbf{z}_t + (1 - \alpha_{t|s}) \mathbf{1} \boldsymbol{\pi}^\top \mathbf{z}_t] \odot [\alpha_s \mathbf{x}_0 + (1 - \alpha_s) \boldsymbol{\pi}]}{\alpha_t \mathbf{z}_t^\top \mathbf{x}_0 + (1 - \alpha_t) \mathbf{z}_t^\top \boldsymbol{\pi}} \right). \quad (2)$$

Of note, for absorbing-state diffusion, where $\boldsymbol{\pi} = [\text{MASK}]$, a one-hot vector at the special [MASK] token index, Sahoo et al. (2024a) show that when the latent $\mathbf{z}_t \neq [\text{MASK}]$ then $q(\mathbf{z}_s | \mathbf{z}_t, \mathbf{x}_0) = \text{Cat}(\mathbf{z}_s; \mathbf{z}_t)$, which reflects the fact that unmasked tokens at time t must remain unmasked for all time $s < t$.

2.2 DIFFUSION GUIDANCE

For continuous data, diffusion models have demonstrated state-of-the-art controllable generation by means of classifier-based (Sohl-Dickstein et al., 2015; Dhariwal & Nichol, 2021a) and classifier-free guidance (Nichol et al., 2021; Ho & Salimans, 2022; Saharia et al., 2022). These approaches rely on different ways of expressing the score of a distribution conditioned on y .

Classifier-based Classifier-based generation employs a diffusion model to iteratively sample from a tempered distribution $p^\gamma(\mathbf{z}_s | y, \mathbf{z}_t) \propto p(y | \mathbf{z}_s)^\gamma p_\theta(\mathbf{z}_s | \mathbf{z}_t)$, where γ represents an inverse temperature parameter, $p_\theta(\mathbf{z}_s | \mathbf{z}_t)$ is a pre-trained diffusion model, and $p(y | \mathbf{z}_s)$ is a classifier:

$$\nabla_{\mathbf{z}_s} \log p^\gamma(\mathbf{z}_s | y, \mathbf{z}_t) = \gamma \nabla_{\mathbf{z}_s} \log p(y | \mathbf{z}_s) + \nabla_{\mathbf{z}_s} \log p_\theta(\mathbf{z}_s | \mathbf{z}_t). \quad (3)$$

Classifier-free We can also observe that applying Bayes' rule to $p(y | \mathbf{x})$ and differentiating with respect to the input yields $\nabla_{\mathbf{x}} \log p(y | \mathbf{x}) = \nabla_{\mathbf{x}} \log p(\mathbf{x} | y) - \nabla_{\mathbf{x}} \log p(\mathbf{x})$. Applying this to $p(y | \mathbf{z}_s)$ and plugging into (3) gives us the formulation for classifier-free guidance:

$$\begin{aligned} \nabla_{\mathbf{z}_s} \log p^\gamma(\mathbf{z}_s | y, \mathbf{z}_t) &= \gamma \cdot [\nabla_{\mathbf{z}_s} \log p_\theta(\mathbf{z}_s | y, \mathbf{z}_t) - \nabla_{\mathbf{x}} \log p_\theta(\mathbf{z}_s | \mathbf{z}_t)] + \nabla_{\mathbf{z}_s} \log p_\theta(\mathbf{z}_s | \mathbf{z}_t) \\ &= \gamma \nabla_{\mathbf{z}_s} \log p_\theta(\mathbf{z}_s | y, \mathbf{z}_t) + (1 - \gamma) \nabla_{\mathbf{z}_s} \log p_\theta(\mathbf{z}_s | \mathbf{z}_t). \end{aligned} \quad (4)$$

where $p_\theta(\mathbf{z}_s | y, \mathbf{z}_t)$ and $p_\theta(\mathbf{z}_s | \mathbf{z}_t)$ represent conditional and unconditionally trained diffusion models, respectively. In practice, this is often implemented by using a single model p_θ and randomly dropping out / masking the conditioner y during training.

The problem with applying guidance to discrete diffusion is that guidance terms are not differentiable with respect to the discrete representations \mathbf{z}_t .

3 GUIDANCE ALGORITHMS FOR DISCRETE DIFFUSION

To alleviate the issue of non-differentiability, we introduce two guidance algorithms for discrete diffusion. As in the continuous case, we formalize the guidance term as a probability $p(y|\mathbf{z})$, where $y \in \{1, \dots, K\}$ is one of K possible classes and Δ^K is the K -simplex defined over these classes.

3.1 CLASSIFIER-FREE GUIDANCE

We refer to the following discrete version of classifier guidance as **D-CFG** for **Discrete Classifier-Free Guidance**. To derive D-CFG, we begin by applying Bayes' Rule:

$$p(\mathbf{z}_s | \mathbf{z}_t, y) = [p(y | \mathbf{z}_s, \mathbf{z}_t) / p(y | \mathbf{z}_t)] p(\mathbf{z}_s | \mathbf{z}_t)$$

As in Section 2.2, we wish to sample from the distribution:

$$p^\gamma(\mathbf{z}_s | \mathbf{z}_t, y) \propto [p(y | \mathbf{z}_s, \mathbf{z}_t) / p(y | \mathbf{z}_t)]^\gamma p(\mathbf{z}_s | \mathbf{z}_t)$$

We now examine the right hand side and again apply Bayes' rule :

$$\left[\frac{p(y | \mathbf{z}_s, \mathbf{z}_t)}{p(y | \mathbf{z}_t)} \right]^\gamma p(\mathbf{z}_s | \mathbf{z}_t) = \left[\frac{p(\mathbf{z}_s | \mathbf{z}_t, y) p(y | \mathbf{z}_t)}{p(\mathbf{z}_s | \mathbf{z}_t) p(y | \mathbf{z}_t)} \right]^\gamma p(\mathbf{z}_s | \mathbf{z}_t) = p(\mathbf{z}_s | \mathbf{z}_t, y)^\gamma p(\mathbf{z}_s | \mathbf{z}_t)^{(1-\gamma)}.$$

In practice, we train a conditional denoising network $p_\theta(\mathbf{z}_s | \mathbf{z}_t, y)$ alongside an unconditional one $p_\theta(\mathbf{z}_s | \mathbf{z}_t)$, both of which are parameterized such that for a sequence of L tokens $\mathbf{z}_s^{(1:L)}$ the probabilities factorize independently across the tokens of the sequence when conditioned on $\mathbf{z}_t^{(1:L)}$. We can thus sample from $p^\gamma(\mathbf{z}_s^{(1:L)} | \mathbf{z}_t^{(1:L)}, y)$ by computing $p_\theta(\mathbf{z}_s^{(1:L)} | \mathbf{z}_t^{(1:L)}, y)^\gamma p_\theta(\mathbf{z}_s^{(1:L)} | \mathbf{z}_t^{(1:L)})^{(1-\gamma)}$, which factorizes independently across tokens, and re-normalizing for each token:

$$p_\theta^\gamma(\mathbf{z}_s^{(1:L)} | \mathbf{z}_t^{(1:L)}, y) = \prod_{\ell=1}^L \frac{1}{Z^{(\ell)}} p_\theta(\mathbf{z}_s^{(\ell)} | \mathbf{z}_t^{(1:L)}, y)^\gamma p_\theta(\mathbf{z}_s^{(\ell)} | \mathbf{z}_t^{(1:L)})^{(1-\gamma)}, \quad (5)$$

where $Z^{(\ell)} = \sum_{\mathbf{z}'_s} p_\theta(\mathbf{z}'_s | \mathbf{z}_t^{(1:L)}, y)^\gamma p_\theta(\mathbf{z}'_s | \mathbf{z}_t^{(1:L)})^{(1-\gamma)}$ is the per-token partition function.

3.2 CLASSIFIER-BASED GUIDANCE

Next, we describe a discrete version of classifier-based guidance: **D-CBG** for **Discrete Classifier-Based Guidance**. Extending classifier-based guidance to diffusion models is difficult because the guiding classifier need not factorize the same as the diffusion denoising network, which would imply that the classifier needs to be evaluated on exponentially many sequence combinations. We resolve this using factorization assumptions on the decoding model and a Taylor expansion trick.

First, we introduce the following additional notation: given $\mathbf{z}^{1:L}$, let $\tilde{\mathcal{Z}}_\ell(\mathbf{z}^{1:L})$ be the set of sequences $\tilde{\mathbf{z}}^{(1:L)}$ for which $\tilde{\mathbf{z}}^{(\ell')} = \mathbf{z}^{(\ell')}$ for all $\ell' \neq \ell$, i.e., the set of sequences that are either the same as or only differ in position ℓ relative to $\mathbf{z}^{(1:L)}$.

To formulate discrete classifier-based guidance, we make the assumption that conditioned on $\mathbf{z}_t^{(1:L)}$, the tempered distribution from which we want to sample $p^\gamma(\mathbf{z}_s^{(1:L)} | \mathbf{z}_t^{(1:L)}, y)$ factorizes independently across tokens. Therefore, we can focus on the tempered distribution of each token $\mathbf{z}_s^{(\ell)}$, for $\ell \in 1, \dots, L$:

$$p^\gamma(\mathbf{z}_s^{(\ell)} | \mathbf{z}_t^{(1:L)}, y) \propto p(y | \mathbf{z}_s^{(\ell)}, \mathbf{z}_t^{(1:L)})^\gamma p(\mathbf{z}_s^{(\ell)} | \mathbf{z}_t^{(1:L)}).$$

In practice, we can sample from $p^\gamma(\mathbf{z}_s^{(\ell)} | \mathbf{z}_t^{(1:L)}, y)$ by training a classifier $p_\phi : \mathcal{V}^L \rightarrow \Delta^K$ on noised latents $\mathbf{z}_t^{(1:L)}$ for $t \in [0, 1]$ and use this to model the first term on the right hand side by only evaluating p_ϕ on sequences for which $\mathbf{z}_s^{(1:L)}$ and $\mathbf{z}_t^{(1:L)}$ differ by at most the token at position ℓ :

$$p(y | \mathbf{z}_s^{(\ell)}, \mathbf{z}_t^{(1:L)}) \approx p_\phi(y | \tilde{\mathbf{z}}^{(1:L)}), \quad \text{for } \tilde{\mathbf{z}}^{(1:L)} = [\mathbf{z}_t^{(1:\ell-1)}, \mathbf{z}_s^{(\ell)}, \mathbf{z}_t^{(\ell+1:L)}] \in \tilde{\mathcal{Z}}_\ell(\mathbf{z}_t^{(1:L)}).$$

We additionally train an unconditional denoising network $p_\theta(\mathbf{z}_s^{(\ell)} | \mathbf{z}_t^{(1:L)})$ and then sample from the re-normalized distribution:

$$p_{\phi, \theta}^\gamma(\mathbf{z}_s^{(\ell)} | \mathbf{z}_t^{(1:L)}, y) = \frac{p_\phi(y | \tilde{\mathbf{z}}^{(1:L)})^\gamma p_\theta(\mathbf{z}_s^{(\ell)} | \mathbf{z}_t^{(1:L)})}{\sum_{\tilde{\mathbf{z}}^{(1:L)}} p_\phi(y | \tilde{\mathbf{z}}^{(1:L)})^\gamma p_\theta(\mathbf{z}_s^{(\ell)} | \mathbf{z}_t^{(1:L)})}. \quad (6)$$

Restricting the summation in the denominator of (6) to $\tilde{\mathcal{Z}}_\ell(\mathbf{z}_t^{(1:L)})$ makes normalization tractable, as we are only summing over N terms.

Our method can be thought of as an adaptation of the successful FUDGE (Yang & Klein, 2021) approach, which guides AR generation, to discrete diffusion, similar to how NOS (Gruver et al., 2024) extended the AR guidance mechanism of PPLM (Dathathri et al., 2019) to diffusion models.

First-Order Approximation While tractable, this formulation suffers from the drawback that at each denoising step we must perform $\mathcal{O}(L \cdot N)$ forward passes through the classifier model, which can quickly become impractical for larger vocabularies. Similarly to Grathwohl et al. (2021), Vignac et al. (2022), and Nisonoff et al. (2024), we treat the classifier p_ϕ as a continuous function of the one-hot inputs $\tilde{\mathbf{z}}^{(1:L)} \in \mathbb{R}^{L \times N}$ and use the first-order Taylor approximation of $\log p_\phi$ to efficiently compute $p_\phi(y | \mathbf{z}_s^{(\ell)})$ with only a single forward and backward pass through the classifier model:

$$\begin{aligned} p_\phi(y | \tilde{\mathbf{z}}^{(1:L)}) &= \exp \left(\log \frac{p_\phi(y | \tilde{\mathbf{z}}^{(1:L)})}{p_\phi(y | \mathbf{z}_t^{(1:L)})} + \log p_\phi(y | \mathbf{z}_t^{(1:L)}) \right) \\ &\approx \exp \left((\tilde{\mathbf{z}}^{(1:L)} - \mathbf{z}_t^{(1:L)})^T \nabla_{\mathbf{z}_t^{(1:L)}} \log p_\phi(y | \mathbf{z}_t^{(1:L)}) + \log p_\phi(y | \mathbf{z}_t^{(1:L)}) \right). \quad (7) \end{aligned}$$

4 UNIFORM DIFFUSION LANGUAGE MODELS

While masked diffusion models demonstrate better language modeling compared to other discrete diffusion (Austin et al., 2021; Lou et al., 2023), we argue that they are less amenable to guidance, since once a token is unmasked at some time t it remains so for all $s < t$. In contrast, with uniform noising, intermediate latents can be refined multiple times throughout the denoising process.

We therefore revisit categorical uniform noise discrete diffusion, where $\boldsymbol{\pi} = \mathbf{u} = \mathbf{1}/N$. Our aim is that by analyzing this class of diffusion models more carefully, we can reduce the gap to absorbing-state and yield performant models that are more easily steered by guidance tools we develop below.

4.1 UNIFORM NOISE DIFFUSION

We begin by introducing the background and formulation for interpolating discrete diffusion models with uniform noise.

Discrete Time Likelihood Bound We start with the variational lower bound that is defined by a diffusion process. For discrete time diffusion, i.e., some finite steps T , we define $t(i) = (i + 1)/T$

and $s(i) = i/T$ for i in $0, \dots, T$. The denoising network p_θ is trained to minimize a variational upper bound (NELBO), which is given by:

$$\mathbb{E}_q \left[\underbrace{-\log p_\theta(\mathbf{x}_0 | \mathbf{z}_{t(0)})}_{\mathcal{L}_{\text{recons}}} + \underbrace{\sum_{i=1}^T D_{\text{KL}}[q(\mathbf{z}_{s(i)} | \mathbf{z}_{t(i)}, \mathbf{x}_0) \| p_\theta(\mathbf{z}_{s(i)} | \mathbf{z}_{t(i)})]}_{\mathcal{L}_{\text{diffusion}}} \right] + \underbrace{D_{\text{KL}}[q(\mathbf{z}_{t(T)} | \mathbf{x}_0) \| p_\theta(\mathbf{z}_{t(T)})]}_{\mathcal{L}_{\text{prior}}}, \quad (8)$$

where D_{KL} represents the Kullback-Leibler divergence. When clear, we drop the explicit dependence of t and s on the discrete step i .

Uniform Noise Forward Process We formulate uniform noise diffusion using the interpolating discrete diffusion framework (Sahoo et al., 2024a; Zhao et al., 2024; Zheng et al., 2023). When letting $\pi = \mathbf{u}$, the input \mathbf{x} transitions to a random state with some probability at each time step. Crucially, after \mathbf{x} changes once, it can do so again. When $\pi = \mathbf{u}$, the posterior from (2) becomes

$$q(\mathbf{z}_s | \mathbf{z}_t, \mathbf{x}_0) = \text{Cat} \left(\mathbf{z}_s; \frac{N\alpha_t \mathbf{z}_t \odot \mathbf{x}_0 + (\alpha_{t|s} - \alpha_t) \mathbf{z}_t + (\alpha_s - \alpha_t) \mathbf{x}_0 + \frac{(\alpha_s - \alpha_t)(1 - \alpha_s)}{N\alpha_s} \mathbf{1}}{N\alpha_t \langle \mathbf{z}_t, \mathbf{x}_0 \rangle + 1 - \alpha_t} \right) \quad (9)$$

Denoising Process The optimal form for the reverse diffusion process p_θ matches (9): in fact setting p_θ to (9) reduces the KL terms in (8) to zero. However, setting p_θ to exactly (9) is not possible because it cannot be a function \mathbf{x}_0 (which p_θ is generating). Therefore, we introduce a predictive model $\mathbf{x}_\theta(\mathbf{z}_t, t) : \mathcal{V} \times [0, 1] \rightarrow \Delta^N$ of the ‘clean’ data given a noisy latent \mathbf{z}_t at time t . We use \mathbf{x}_θ to parameterize the denoising process as $p_\theta(\mathbf{z}_s | \mathbf{z}_t) = q(\mathbf{z}_s | \mathbf{z}_t, \mathbf{x} = \mathbf{x}_\theta)$, yielding:

$$p_\theta(\mathbf{z}_s | \mathbf{z}_t) = \text{Cat} \left(\mathbf{z}_s; \frac{N\alpha_t \mathbf{z}_t \odot \mathbf{x}_\theta + (\alpha_{t|s} - \alpha_t) \mathbf{z}_t + (\alpha_s - \alpha_t) \mathbf{x}_\theta + \frac{(\alpha_s - \alpha_t)(1 - \alpha_s)}{N\alpha_s} \mathbf{1}}{N\alpha_t \langle \mathbf{z}_t, \mathbf{x}_\theta \rangle + 1 - \alpha_t} \right), \quad (10)$$

Note that this minimizes the $\mathcal{L}_{\text{diffusion}}$ term in (8) precisely when $\mathbf{x}_\theta = \mathbf{x}_0$, as desired. To simplify notation, we omit below the explicit dependence of \mathbf{x}_θ on t .

4.2 IMPROVED LIKELIHOOD BOUNDS IN CONTINUOUS TIME

We now present our contribution to uniform noise discrete diffusion modeling. We leverage the above formulation to develop an improved ELBO by taking $T \rightarrow \infty$ and analyzing each term $\mathcal{L}_{\text{recons}}$, $\mathcal{L}_{\text{diffusion}}$, $\mathcal{L}_{\text{prior}}$ in (8). This yields three improvements: (1) a simple and elegant closed-form expression for the ELBO that is easier to reason about; (2) an analytical reduction of $\mathcal{L}_{\text{recons}}$, $\mathcal{L}_{\text{prior}}$ to zero, which tightens the ELBO; (3) a further tightening via the continuous-time extension of $\mathcal{L}_{\text{diffusion}}$ as in Kingma et al. (2021) and Sahoo et al. (2024a;b).

Prior Loss ($\mathcal{L}_{\text{prior}}$) Given that we define our corruption process as an interpolation between clean data and a limiting distribution, for any noise schedules where $\alpha_{t(T)} = 0$, the distribution $q(\mathbf{z}_{t(T)}) = \pi$. Therefore, we can simply define $p_\theta(\mathbf{z}_{t(T)}) = \pi$, and the KL divergence in $\mathcal{L}_{\text{prior}}$ evaluates to zero.

Reconstruction Loss ($\mathcal{L}_{\text{recons}}$) Similarly, for $\mathcal{L}_{\text{recons}}$, if our noise schedule is such that $T \rightarrow \infty \implies \alpha_{t(0)} = 1$ (i.e., $t(0) = 1/T$), then the marginal $q(\mathbf{z}_{\frac{1}{T}} | \mathbf{x}_0) \rightarrow \text{Cat}(\mathbf{z}_{\frac{1}{T}}; \mathbf{x}_0)$. That is, in the limit, the first latent vector is identically equal to the clean data. We can thus parameterize our denoising network such that at time $t(0)$ the function simply copies its inputs: $\mathbf{x}_\theta(\mathbf{z}_{\frac{1}{T}}, 1/T) = \mathbf{z}_{\frac{1}{T}}$. Additionally, we note that our choice of parameterization for p_θ implies that $p_\theta(\mathbf{x}_0 | \mathbf{z}_{\frac{1}{T}}) = \mathbf{x}_\theta(\mathbf{z}_{\frac{1}{T}}, 1/T)$. Thus in the continuous time limit, we have:

$$\lim_{T \rightarrow \infty} \mathbb{E}_q[\mathcal{L}_{\text{recons}}] = \lim_{T \rightarrow \infty} \mathbb{E}_q[\log p_\theta(\mathbf{x}_0 | \mathbf{z}_{\frac{1}{T}})] = \lim_{T \rightarrow \infty} \mathbb{E}_q[\log(\langle \mathbf{x}_0, \mathbf{x}_\theta(\mathbf{z}_{\frac{1}{T}}, 1/T) \rangle)] = 0.$$

Diffusion Loss ($\mathcal{L}_{\text{diffusion}}$) Turning finally to the diffusion loss term $\mathcal{L}_{\text{diffusion}}$, we first define the shorthand $D_{\text{KL}}[q_t \| p_\theta] = D_{\text{KL}}[q(\mathbf{z}_s | \mathbf{z}_t, \mathbf{x}_0) \| p_\theta(\mathbf{z}_s | \mathbf{z}_t)]$ and then re-write this term as an expectation over t uniformly sampled from $1/T, 2/T, \dots, T$:

$$\mathcal{L}_{\text{diffusion}} = \sum_{i=1}^T D_{\text{KL}}[q_{i/T} \| p_\theta] = T \cdot \mathbb{E}_{t \sim \{1/T, 2/T, \dots, T\}} D_{\text{KL}}[q_t \| p_\theta]. \quad (11)$$

Plugging in our expressions for the true and predicted posteriors from (9) and (10) into (11), then taking $T \rightarrow \infty$, we get (see Appendix A for details):

$$\begin{aligned} \lim_{T \rightarrow \infty} \mathcal{L}_{\text{diffusion}} &= \lim_{T \rightarrow \infty} \mathbb{E}_{t \sim \{1/T, 2/T, \dots, T\}} T \cdot D_{\text{KL}}[q_t || p_\theta] = \int_{t=0}^{t=1} \lim_{T \rightarrow \infty} T \cdot D_{\text{KL}}[q_t || p_\theta] dt \\ &= \int_{t=0}^{t=1} \left[\frac{\alpha'_t}{N\alpha_t} \left[\frac{N}{\bar{\mathbf{x}}_i} - \frac{N}{(\bar{\mathbf{x}}_\theta)_i} - \sum_{j \text{ s.t. } (\mathbf{z}_t)_j=0} \left(\frac{\bar{\mathbf{x}}_j}{\bar{\mathbf{x}}_i} \right) \log \left[\left(\frac{(\bar{\mathbf{x}}_\theta)_i \cdot \bar{\mathbf{x}}_j}{(\bar{\mathbf{x}}_\theta)_j \cdot \bar{\mathbf{x}}_i} \right) \right] \right] \right] dt, \end{aligned} \quad (12)$$

where \mathbf{x}_i denotes the i^{th} index of a vector \mathbf{x} , $\bar{\mathbf{x}} = N\alpha_t\mathbf{x} + (1 - \alpha_t)\mathbf{1}$, $\bar{\mathbf{x}}_\theta = N\alpha_t\mathbf{x}_\theta + (1 - \alpha_t)\mathbf{1}$, and we define $i = \arg \max_{j \in [N]} (\mathbf{z}_t)_j$ to be the non-zero entry of \mathbf{z}_t .

Combining our arguments regarding $\mathcal{L}_{\text{prior}}$ and $\mathcal{L}_{\text{recons}}$ with (12), yields our final tight variational bound:

$$\mathcal{L}^\infty = \int_{t=0}^{t=1} \mathbb{E}_q \left[\frac{\alpha'_t}{N\alpha_t} \left[\frac{N}{\bar{\mathbf{x}}_i} - \frac{N}{(\bar{\mathbf{x}}_\theta)_i} - \sum_{j \text{ s.t. } (\mathbf{z}_t)_j=0} \left(\frac{\bar{\mathbf{x}}_j}{\bar{\mathbf{x}}_i} \right) \log \left[\left(\frac{(\bar{\mathbf{x}}_\theta)_i \cdot \bar{\mathbf{x}}_j}{(\bar{\mathbf{x}}_\theta)_j \cdot \bar{\mathbf{x}}_i} \right) \right] \right] \right] dt. \quad (13)$$

Extension to Sequences Extending training with (13) from $\mathbf{x} \in \mathcal{V}$ to sequences $\mathbf{x}^{(1:L)} \in \mathcal{V}^L$, we make the assumption that the denoising process factorizes independently across tokens when conditioned on a sequence of noisy latents $\mathbf{z}_t^{(1:L)}$. In this case, we use a single model $\mathbf{x}_\theta^{(\ell)}(\mathbf{z}_t^{(1:L)}, t)$ for predicting each token $\ell \in \{1, \dots, L\}$ in a sequence, and we train with the sequence-level objective:

$$\mathcal{L}^\infty = \int_{t=0}^{t=1} \mathbb{E}_q \sum_{\ell} \left[\frac{\alpha'_t}{N\alpha_t} \left[\frac{N}{\bar{\mathbf{x}}_i^{(\ell)}} - \frac{N}{(\bar{\mathbf{x}}_\theta)_i^{(\ell)}} - \sum_{j \text{ s.t. } (\mathbf{z}_t^{(\ell)})_j=0} \left(\frac{\bar{\mathbf{x}}_j^{(\ell)}}{\bar{\mathbf{x}}_i^{(\ell)}} \right) \log \left[\left(\frac{(\bar{\mathbf{x}}_\theta)_i^{(\ell)} \cdot \bar{\mathbf{x}}_j^{(\ell)}}{(\bar{\mathbf{x}}_\theta)_j^{(\ell)} \cdot \bar{\mathbf{x}}_i^{(\ell)}} \right) \right] \right] \right] dt. \quad (14)$$

We dub models trained with our refined objective **Uniform Diffusion Language Models (UDLM)**.

5 EXPERIMENTS

Datasets For our language modeling experiments we examine several distinct discrete domains: reference genomes from ten diverse species (Species-10), the small molecule dataset known as QM9 (Ruddigkeit et al., 2012; Ramakrishnan et al., 2014), where molecules are represented by a string of characters known as SMILES (Weininger, 1988), discretized images from CIFAR-10 (Krizhevsky et al., 2009), and three NLP datasets consisting of text8 (Mahoney, 2011), Amazon Review Polarity (McAuley & Leskovec, 2013; Zhang et al., 2015), and the one billion words dataset (LM1B; Chelba et al. (2014)). These datasets cover a range of domains and vocabularies of varying sizes (see Table 1). For guidance experiments, we explore species-specific sequence generation, molecular property maximization, and class-conditional image generation.

5.1 LANGUAGE MODELING WITH UNIFORM NOISE DISCRETE DIFFUSION

Our language modeling experiments reveal that (1) contrary to a widely-held belief, **uniform noise diffusion can attain state-of-the-art performance** on small vocabulary datasets (Table 1), and that (2) our **UDLM are state-of-the-art among uniform noise diffusion models** (Tables 2 and 3).

In Table 1, despite previous evidence indicating that absorbing-state discrete diffusion greatly outperforms uniform noise, we find a more nuanced story. Namely, for smaller vocabulary regimes, which are common for scientific applications, the gap between MDLM and UDLM is negligible, with UDLM even outperforming absorbing-state diffusion on certain datasets. Even within a single domain, we find a trend between vocabulary size and performance gap, with the text8 results of UDLM on par with MDLM, and a more persistent gap for the larger vocabulary experiments. Intuitively, these results follow from the observation that in larger vocabulary regimes, at every denoising step, uniform noise diffusion models need to predict over a combinatorially larger set of potential clean data sequences compared to absorbing-state; smaller vocabularies reduce this complexity.

Secondly, although we still find a persisting perplexity gap between absorbing and uniform noise discrete diffusion for larger vocabulary NLP datasets, we note that our uniform noise diffusion models trained with UDLM, closes this gap, as evidenced in Tables 2 and 3, where we show that UDLM attains the best reported uniform noise discrete diffusion language modeling performance.

Table 1: UDLM performs best in smaller vocabulary regimes. Values correspond to perplexity (PPL; \downarrow) on various datasets. Best values are **bolded**. Datasets marked with * have values reported from early stopping on the validation set, since AR model demonstrated overfitting; Values for all other datasets reflect validation performance at the end of training. [†]Taken from Sahoo et al. (2024a). [§]Taken from Lou et al. (2023).

		Vocab. Size	AR	MDLM	UDLM
<i>Bio.</i>	Species-10	12	2.88	3.17 _{<}	3.15 _{<}
<i>Chem.</i>	QM9*	40	2.19	2.12 _{<}	2.02 _{<}
<i>Images</i>	CIFAR-10	256	-	9.14 _{<}	11.21 _{<}
<i>NLP</i>	text8	35	2.35 [§]	2.62 _{<}	2.71 _{<}
	Amazon*	30,522	21.67	24.93 _{<}	27.27 _{<}
	LM1B	30,522	22.32 [†]	27.04 _{<} [†]	31.28 _{<}

Table 2: UDLM outperforms previously reported uniform noise discrete diffusion models on text8 dataset. Values correspond to bits per character (BPC). Best values are **bolded** and best discrete uniform diffusion value is underlined. [†]Taken from Lou et al. (2023).

Method	BPC (\downarrow)
<i>Autoregressive</i> [†]	
IAF/SCF	1.88
AR Argmax Flow	1.39
Discrete Flow	1.23
Autoregressive	1.23
<i>Non-autoregressive</i> [†]	
Mult. Diffusion	1.72 _{<}
MAC	1.40 _{<}
BFN	1.41 _{<}
D3PM Absorb	1.45 _{<}
SEDD Absorb	1.39 _{<}
MDLM	1.38 _{<}
<i>Discrete Uniform Diffusion</i>	
D3PM Uniform [†]	1.61 _{<}
SEDD Uniform [†]	1.47 _{<}
UDLM (<i>Ours</i>)	<u>1.44</u> _{<}

Table 3: UDLM outperforms previously reported uniform noise discrete diffusion models on LM1B dataset. Values correspond to perplexity (PPL). Best values are **bolded** and best discrete uniform diffusion value is underlined. [†]Taken from Sahoo et al. (2024a). ^{*}Taken from Lou et al. (2023). [§]Taken from Austin et al. (2021).

Method	PPL (\downarrow)
<i>Autoregressive</i> [†]	
Transformer-X Base	23.5
OmniNetT	21.5
Transformer	22.32
<i>Diffusion</i> [†]	
BERT-Mouth	142.89 _{<}
D3PM Absorb	77.50 _{<}
Diffusion-LM	118.62 _{<}
DiffusionBert	63.78 _{<}
SEDD Absorb	32.79 _{<}
MDLM	27.04 _{<}
<i>Discrete Uniform Diffusion</i>	
D3PM Uniform [§]	137.9 _{<}
SEDD Uniform*	40.25 _{<}
UDLM (<i>Ours</i>)	<u>31.28</u> _{<}

Ablating Continuous Time Formulation In Figure 1, we see the effect of increasing T and more specifically using our continuous time ELBO. The curves represent validation perplexity on the Amazon Polarity dataset at various training steps, and we observe that increasing T indeed improves language modeling with UDLM, i.e., $T = \infty$, performing best.

5.2 GUIDED DISCRETE DIFFUSION

Our guidance results indicate that (1) **classifier-free guidance is more useful when paired with diffusion models compared to AR** (Table 4) and that (2) **our proposed D-CBG is the best classifier-based method** for discrete guidance, especially when combined with UDLM (Tables 5 and 6).

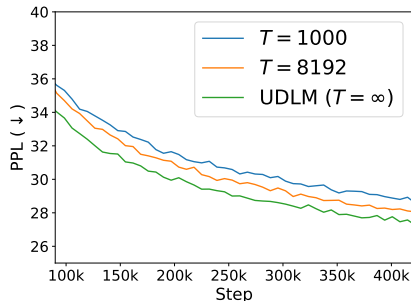


Figure 1: Increasing T to infinity improves language modeling. Values correspond to validation perplexity (PPL) for uniform noise discrete diffusion using finite T vs. UDLM ($T = \infty$).

Table 4: Diffusion decoding is more controllable than AR for genomic sequences. Best values are **bolded**.

Model	Guidance	3-mer JS (\downarrow)	6-mer JS (\downarrow)	Disc. AUROC (\downarrow)	F1 (\uparrow)
Random	-	0.13	0.22	1.00	0.07
AR	D-CFG $_{\gamma=1}$	0.04	0.09	1.00	0.87
AR	D-CFG $_{\gamma=2}$	0.05	0.14	1.00	0.68
MDLM	D-CFG $_{\gamma=1}$	0.03	0.07	0.61	0.90
MDLM	D-CFG $_{\gamma=2}$	0.04	0.11	0.71	0.78
UDLM	D-CFG $_{\gamma=1}$	0.03	0.08	0.77	0.92
UDLM	D-CFG $_{\gamma=2}$	0.08	0.18	0.75	0.96

Baselines For guidance experiments, our primary baseline is the dominant approach for language modeling, AR. Our goal is to show that with similar, even slightly worse, language modeling performance, discrete diffusion models equipped with classifier-based and classifier-free guidance can outperform AR models on controlled generation. We compare to three flavors of guided AR models. The first is applying D-CFG to AR models. We also use the established control mechanisms of Plug-and-play language models (PPLM; Dathathri et al. (2019)) and FUDGE (Yang & Klein, 2021). To demonstrate the better performance of our D-CBG method, we compare to Gruver et al. (2024) (NOS) which can be viewed as an extension of PPLM to discrete diffusion models.

Hyperparameters For both our D-CFG and D-CBG methods we vary the strength of the γ parameter. Although the original FUDGE formulation simply uses $\gamma = 1$, we also perform a search for this baseline. For PPLM and NOS, we vary the parameters of the Langevin sampling that is performed to update models’ hidden representation, namely the step size η , the fluency KL weight γ_{kl} , and the number of update steps n (see Dathathri et al. (2019) and Gruver et al. (2024) for more details). For all methods, we display the best performing hyperparameter configuration in the main table results, deferring the full sweep results to Appendix D.

Species-specific Genome Generation For genomic sequences, we evaluate D-CFG with diffusion models vs. with an AR model. We train models on sequences of length 32,768 nucleotides, using base-pair level tokenization and conditionally generate 64 sequences for each class. As quality measures for each species class, we compute the Jensen-Shannon (JS) distance between the k -mer frequencies of the generated sequences and those from the validation set, and report the mean JS across species (weighted by species frequency in the dataset), with smaller values indicating better k -mer distributional overlap between the ground truth and generated sequences (Sarkar et al., 2024). Additionally, we train a small classifier to distinguish between generated and validation set sequences and report the area under the receiver operator curve for this classifier (Disc. AUROC). Values closer to 0.5 indicate that the classifier is unable to distinguish between synthetic and true sequences (Sarkar et al., 2024). To measure the controllability, we train a separate classifier on the Species-10 dataset and measure macro F1 score of this oracle classifier on the generated sequences.

Results of this experiment are presented in Table 4. For reference, we also provide metrics for randomly generating sequences with nucleotide frequencies proportional to each species’ validation subset. We find that both MDLM and UDLM are able to better generate sequences that match the desired control parameter, with higher F1 scores under the evaluation oracle relative to AR. Moreover, UDLM is able to outperform MDLM in satisfying this control. Importantly, we find that only UDLM is amenable to increasing the guidance parameter γ , where its metrics improves while AR and MDLM metrics degrade.

Finally, of note, the diffusion model generation for this experiment is accomplished with far fewer function evaluations compared to AR. Whereas AR must decode each of the 32,768 tokens, because MDLM and UDLM can decode multiple tokens in parallel, we generate with $T = 512$.

Molecular Property Maximization For the QM9 dataset, we investigate novel generation of sequences that maximize some property, either drug-likeness (QED; Bickerton et al. (2012)), see Table 5, or a count of the number of rings present in the molecule, see Table 6.

For D-CFG, we see that all methods perform comparably when maximizing drug likeness, but that UDLM is better suited towards guidance for the structural property of ring count, as it achieves similar property maximization to AR and MDLM, without sacrificing the validity and novelty of generated sequences. This pattern is even more evident when examining classifier-based guidance mechanisms, where we find that for both QED and ring count, UDLM best trades-off maximizing these properties while generating sensible and not memorized sequences.

Table 5: Guidance with discrete diffusion models better balances the generation of valid and novel molecules with maximizing the property of interest, drug likeness (QED), compared to AR. Validity, novelty, and mean QED for novel sequences are measured for generated sequences from each method. Best values are **bolded**.

Method	Guidance	Valid (\uparrow)	Novel (\uparrow)	QED Mean (\uparrow)
Original Data	-	133k	133k	0.47
<i>Classifier-free</i>				
AR	D-CFG $_{\gamma=2.5}$	1995	130	0.60
MDLM	D-CFG $_{\gamma=3.0}$	652	251	0.61
UDLM	D-CFG $_{\gamma=3.0}$	2034	133	0.61
<i>Classifier-based</i>				
AR	FUDGE $_{\gamma=10}$	914	24	0.58
AR	PPLM $_{\eta=0.1, n=30}$	1618	291	0.48
MDLM	D-CBG $_{\gamma=20}$ (Ours)	64	22	0.58
MDLM	NOS $_{\eta=0.001, n=1, \gamma_{kl}=0.01}$	1302	471	0.45
UDLM	D-CBG $_{\gamma=35}$ (Ours)	1223	87	0.61
UDLM	NOS $_{\eta=5, n=5, \gamma_{kl}=0.001}$	946	302	0.47

Table 6: Guidance with UDLM best balances the generation of valid and novel molecules with maximizing the property of interest, ring count, compared to AR and MDLM. Validity, novelty, and mean ring count for novel sequences are measured for generated sequences from each method. Best values are **bolded**.

Method	Guidance	Valid (\uparrow)	Novel (\uparrow)	Ring Count Mean (\uparrow)
Original Data	-	133k	133k	1.74
<i>Classifier-free</i>				
AR	D-CFG $_{\gamma=7.0}$	108	24	5.04
MDLM	D-CFG $_{\gamma=6.0}$	132	90	5.01
UDLM	D-CFG $_{\gamma=3.5}$	1975	459	4.91
<i>Classifier-based</i>				
AR	FUDGE $_{\gamma=2}$	2035	15	4.20
AR	PPLM $_{\eta=0.1, n=30}$	1486	233	1.89
MDLM	D-CBG $_{\gamma=25}$ (Ours)	82	65	5.05
MDLM	NOS $_{\eta=5, n=10, \gamma_{kl}=0.01}$	353	246	3.31
UDLM	D-CBG $_{\gamma=40}$ (Ours)	1670	943	4.73
UDLM	NOS $_{\eta=5, n=10, \gamma_{kl}=0.01}$	961	402	2.64

Class-conditional Image Generation In Table 7, we see the positive effect of guided-generation on image quality. Both MDLM and UDLM outperform their finite-time counterparts (in the form of D3PM (Austin et al., 2021)) and, moreover, generating with D-CFG ($\gamma = 4$) further improves the image quality metrics of Fréchet inception distance (FID; Heusel et al. (2017)) and Inception Score (IS; Salimans et al. (2016)). In Figure 2, we show several conditionally generated images.

Table 7: Guidance improves image on discretized CIFAR-10. FID and IS for finite- (D3PM) and continuous-time (MDLM / UDLM) discrete diffusion models. Guidance using D-CFG ($\gamma = 4$). Best values are **bolded**. [†]Taken from Austin et al. (2021).

	FID (\downarrow)	IS (\uparrow)
D3PM Absorb [†]	41.28	6.26
MDLM	33.75	6.74
MDLM D-CFG	15.56	9.02
D3PM Uniform [†]	51.27	5.99
UDLM	33.65	6.86
UDLM D-CFG	23.21	8.66

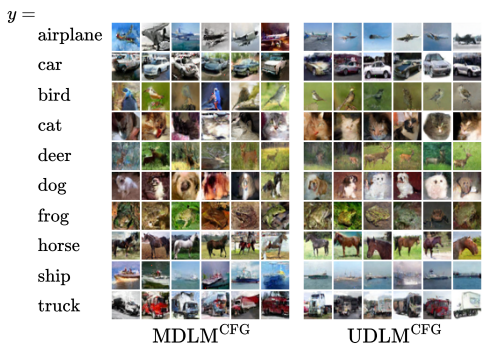


Figure 2: Conditionally generated images for each class in CIFAR10.

6 RELATED WORKS, DISCUSSION, AND CONCLUSION

Discrete Diffusion Our UDLM method most closely aligns to the recent state-of-the-art discrete diffusion models of Ou et al. (2024), Sahoo et al. (2024a), and Shi et al. (2024) that focus on absorbing state diffusion. Similar to these works, we provide a continuous time ELBO leading to performance gains, but we focus on uniform noise. Of note, other extensions of D3PM that do not start from the variational perspective, instead rely on the formalisms of continuous time Markov chains (CTMC) (Campbell et al., 2022) and concrete score matching (Lou et al., 2023), but are less performant than works such as MDLM (Sahoo et al., 2024a) and our method.

Guidance Leveraging continuous embeddings of discrete data, Diffusion-LM (Li et al., 2022) uses Langevin sampling with classifier-based guidance. Similarly, SSD-LM (Han et al., 2022) perform Gaussian noising on the logits of a bi-directional model, which they combine with pre-trained classifiers to perform classifier-based guidance with Langevin dynamics. LD4LG (Lovell et al., 2024) implement classifier-free guidance on continuous embeddings. Wang et al. (2023) perform guidance using auxiliary semantic latent variables. In contrast, to these continuous formulations for discrete data, our work adapts guidance mechanisms directly to the discrete domain.

FUDGE (Yang & Klein, 2021) can be viewed an analog to our D-CBG, but is restricted to AR parameterizations of the denoising network. DiGress (Vignac et al., 2022) uses a similar first-order approximation to the one we employ. However, in DiGress this approximation is used to resolve the intractability of the normalizing constant. In our work, we derive a tractable expression for classifier-based guidance and simply use the Taylor approximation to speed up computation in large sequence length and vocabulary size regimes.

Sanchez et al. (2023) derives an equivalent formulation for D-CFG and use it to better enforce AR models’ adherence to prefix prompts. FreeGress (Ninniri et al., 2024) also offer a comparable method to D-CFG, but focus on graph diffusion models. Most similar to our method, is the concurrent work of Nisonoff et al. (2024), which derives classifier-based and classifier-free guidance for diffusion and flow models. However, this work is highly tailored to models that leverage formalism of continuous time Markov chains and guidance is applied to the rate matrices.

Conclusion In search of a more controllable diffusion process, in this work, we derived a tight variational bound for uniform noise discrete diffusion, closing the gap to state-of-the-art absorbing-state diffusion models. We also highlighted that contrary to previous findings, in small vocabulary regimes, uniform noise is on par or better than absorbing state.

We then demonstrated that straightforward adaptations of classifier-based and classifier-free guidance can offer improved guided generation relative to AR models. We found that with classifier-free mechanisms, diffusion models are more amenable to control without sacrificing quality of generated sequences. We also demonstrated that our classifier-based method is better than previous ones for both AR and diffusion models and is best paired with our UDLM.

REFERENCES

- 540
541
542 Jacob Austin, Daniel D Johnson, Jonathan Ho, Daniel Tarlow, and Rianne Van Den Berg. Structured
543 denoising diffusion models in discrete state-spaces. *Advances in Neural Information Processing*
544 *Systems*, 34:17981–17993, 2021.
- 545 G Richard Bickerton, Gaia V Paolini, Jérémy Besnard, Sorel Muresan, and Andrew L Hopkins.
546 Quantifying the chemical beauty of drugs. *Nature chemistry*, 4(2):90–98, 2012.
- 547 Andrew Campbell, Joe Benton, Valentin De Bortoli, Thomas Rainforth, George Deligiannidis, and
548 Arnaud Doucet. A continuous time framework for discrete denoising models. *Advances in Neural*
549 *Information Processing Systems*, 35:28266–28279, 2022.
- 550
551 Ciprian Chelba, Tomas Mikolov, Mike Schuster, Qi Ge, Thorsten Brants, Phillipp Koehn, and Tony
552 Robinson. One billion word benchmark for measuring progress in statistical language modeling,
553 2014.
- 554 Sumanth Dathathri, Andrea Madotto, Janice Lan, Jane Hung, Eric Frank, Piero Molino, Jason Yosin-
555 ski, and Rosanne Liu. Plug and play language models: A simple approach to controlled text
556 generation. *arXiv preprint arXiv:1912.02164*, 2019.
- 557
558 Prafulla Dhariwal and Alexander Nichol. Diffusion models beat gans on image synthesis. *Advances*
559 *in neural information processing systems*, 34:8780–8794, 2021a.
- 560 Prafulla Dhariwal and Alexander Nichol. Diffusion models beat gans on image synthesis. *Advances*
561 *in neural information processing systems*, 34:8780–8794, 2021b.
- 562
563 Ruiqi Gao, Aleksander Holynski, Philipp Henzler, Arthur Brussee, Ricardo Martin-Brualla, Pratul
564 Srinivasan, Jonathan T. Barron, and Ben Poole. Cat3d: Create anything in 3d with multi-view
565 diffusion models, 2024. URL <https://arxiv.org/abs/2405.10314>.
- 566 Aaron Gokaslan, A Feder Cooper, Jasmine Collins, Landan Seguin, Austin Jacobson, Mihir Patel,
567 Jonathan Frankle, Cory Stephenson, and Volodymyr Kuleshov. Commoncanvas: Open diffusion
568 models trained on creative-commons images. In *Proceedings of the IEEE/CVF Conference on*
569 *Computer Vision and Pattern Recognition*, pp. 8250–8260, 2024.
- 570 Will Grathwohl, Kevin Swersky, Milad Hashemi, David Duvenaud, and Chris Maddison. Oops
571 i took a gradient: Scalable sampling for discrete distributions. In *International Conference on*
572 *Machine Learning*, pp. 3831–3841. PMLR, 2021.
- 573
574 Nate Gruver, Samuel Stanton, Nathan Frey, Tim GJ Rudner, Isidro Hotzel, Julien Lafrance-Vanasse,
575 Arvind Rajpal, Kyunghyun Cho, and Andrew G Wilson. Protein design with guided discrete
576 diffusion. *Advances in neural information processing systems*, 36, 2024.
- 577 Albert Gu and Tri Dao. Mamba: Linear-time sequence modeling with selective state spaces. *arXiv*
578 *preprint arXiv:2312.00752*, 2023.
- 579
580 Xiaochuang Han, Sachin Kumar, and Yulia Tsvetkov. Ssd-lm: Semi-autoregressive simplex-
581 based diffusion language model for text generation and modular control. *arXiv preprint*
582 *arXiv:2210.17432*, 2022.
- 583 Martin Heusel, Hubert Ramsauer, Thomas Unterthiner, Bernhard Nessler, and Sepp Hochreiter.
584 Gans trained by a two time-scale update rule converge to a local nash equilibrium. *Advances in*
585 *neural information processing systems*, 30, 2017.
- 586 Jonathan Ho and Tim Salimans. Classifier-free diffusion guidance. *arXiv preprint*
587 *arXiv:2207.12598*, 2022.
- 588
589 Jonathan Ho, Ajay Jain, and Pieter Abbeel. Denoising diffusion probabilistic models. *Advances in*
590 *neural information processing systems*, 33:6840–6851, 2020.
- 591 Frank P Kelly. *Reversibility and stochastic networks*. Cambridge University Press, 2011.
- 592
593 Diederik Kingma, Tim Salimans, Ben Poole, and Jonathan Ho. Variational diffusion models. *Ad-*
vances in neural information processing systems, 34:21696–21707, 2021.

- 594 Alex Krizhevsky, Geoffrey Hinton, et al. Learning multiple layers of features from tiny images.
595 2009.
- 596
- 597 Greg Landrum et al. Rdkit: A software suite for cheminformatics, computational chemistry, and
598 predictive modeling. *Greg Landrum*, 8(31.10):5281, 2013.
- 599
- 600 Xiang Li, John Thickstun, Ishaan Gulrajani, Percy S Liang, and Tatsunori B Hashimoto. Diffusion-
601 lm improves controllable text generation. *Advances in Neural Information Processing Systems*,
602 35:4328–4343, 2022.
- 603 Aaron Lou, Chenlin Meng, and Stefano Ermon. Discrete diffusion language modeling by estimating
604 the ratios of the data distribution. *arXiv preprint arXiv:2310.16834*, 2023.
- 605
- 606 Justin Lovelace, Varsha Kishore, Chao Wan, Eliot Shekhtman, and Kilian Q Weinberger. Latent
607 diffusion for language generation. *Advances in Neural Information Processing Systems*, 36, 2024.
- 608
- 609 Matt Mahoney. Text8 dataset, 2011. URL <http://mattmahoney.net/dc/textdata>.
- 610
- 611 Julian McAuley and Jure Leskovec. Hidden factors and hidden topics: understanding rating dimen-
612 sions with review text. In *Proceedings of the 7th ACM conference on Recommender systems*, pp.
613 165–172, 2013.
- 614
- 615 Chenlin Meng, Kristy Choi, Jiaming Song, and Stefano Ermon. Concrete score matching: General-
616 ized score matching for discrete data. *Advances in Neural Information Processing Systems*, 35:
617 34532–34545, 2022.
- 618
- 619 Alex Nichol, Prafulla Dhariwal, Aditya Ramesh, Pranav Shyam, Pamela Mishkin, Bob McGrew,
620 Ilya Sutskever, and Mark Chen. Glide: Towards photorealistic image generation and editing with
621 text-guided diffusion models. *arXiv preprint arXiv:2112.10741*, 2021.
- 622
- 623 Matteo Ninniri, Marco Podda, and Davide Bacciu. Classifier-free graph diffusion for molecular
624 property targeting. In *Joint European Conference on Machine Learning and Knowledge Discov-
625 ery in Databases*, pp. 318–335. Springer, 2024.
- 626
- 627 Hunter Nisonoff, Junhao Xiong, Stephan Allenspach, and Jennifer Listgarten. Unlocking guidance
628 for discrete state-space diffusion and flow models. *arXiv preprint arXiv:2406.01572*, 2024.
- 629
- 630 Nuala A O’Leary, Mathew W Wright, J Rodney Brister, Stacy Ciuffo, Diana Haddad, Rich McVeigh,
631 Bhanu Rajput, Barbara Robbertse, Brian Smith-White, Danso Ako-Adjei, Alexander Astashyn,
632 Azat Badretdin, Yiming Bao, Olga Blinkova, Vyacheslav Brover, Vyacheslav Chetvernin, Jinna
633 Choi, Eric Cox, Olga Ermolaeva, Catherine M Farrell, Tamara Goldfarb, Tripti Gupta, Daniel
634 Haft, Eneida Hatcher, Wratko Hlavina, Vinita S Joardar, Vamsi K Kodali, Wenjun Li, Donna Mag-
635 glott, Patrick Masterson, Kelly M McGarvey, Michael R Murphy, Kathleen O’Neill, Shashikant
636 Pujar, Sanjida H Rangwala, Daniel Rausch, Lillian D Riddick, Conrad Schoch, Andrei Shkeda,
637 Susan S Storz, Hanzhen Sun, Francoise Thibaud-Nissen, Igor Tolstoy, Raymond E Tully, An-
638 jana R Vatsan, Craig Wallin, David Webb, Wendy Wu, Melissa J Landrum, Avi Kimchi, Tatiana
639 Tatusova, Michael DiCuccio, Paul Kitts, Terence D Murphy, and Kim D Pruitt. Reference se-
640 quence (RefSeq) database at NCBI: current status, taxonomic expansion, and functional annota-
641 tion. *Nucleic Acids Res.*, 44(D1):D733–45, January 2016.
- 642
- 643 Jingyang Ou, Shen Nie, Kaiwen Xue, Fengqi Zhu, Jiacheng Sun, Zhenguo Li, and Chongxuan
644 Li. Your absorbing discrete diffusion secretly models the conditional distributions of clean data.
645 *arXiv preprint arXiv:2406.03736*, 2024.
- 646
- 647 William Peebles and Saining Xie. Scalable diffusion models with transformers. In *Proceedings of
the IEEE/CVF International Conference on Computer Vision*, pp. 4195–4205, 2023.
- 648
- 649 Ben Poole, Ajay Jain, Jonathan T Barron, and Ben Mildenhall. Dreamfusion: Text-to-3d using 2d
650 diffusion. *arXiv preprint arXiv:2209.14988*, 2022.
- 651
- 652 Raghunathan Ramakrishnan, Pavlo O Dral, Matthias Rupp, and O Anatole Von Lilienfeld. Quantum
653 chemistry structures and properties of 134 kilo molecules. *Scientific data*, 1(1):1–7, 2014.

- 648 Olaf Ronneberger, Philipp Fischer, and Thomas Brox. U-net: Convolutional networks for biomedical
649 image segmentation. In *Medical image computing and computer-assisted intervention—MICCAI 2015: 18th international conference, Munich, Germany, October 5-9, 2015, proceedings, part III 18*, pp. 234–241. Springer, 2015.
- 652 Lars Ruddigkeit, Ruud Van Deursen, Lorenz C Blum, and Jean-Louis Reymond. Enumeration of 166
653 billion organic small molecules in the chemical universe database gdb-17. *Journal of chemical*
654 *information and modeling*, 52(11):2864–2875, 2012.
- 656 Chitwan Saharia, William Chan, Saurabh Saxena, Lala Li, Jay Whang, Emily L Denton, Kamyar
657 Ghasemipour, Raphael Gontijo Lopes, Burcu Karagol Ayan, Tim Salimans, et al. Photorealistic
658 text-to-image diffusion models with deep language understanding. *Advances in neural informa-*
659 *tion processing systems*, 35:36479–36494, 2022.
- 660 Subham Sekhar Sahoo, Marianne Arriola, Yair Schiff, Aaron Gokaslan, Edgar Marroquin, Justin T
661 Chiu, Alexander Rush, and Volodymyr Kuleshov. Simple and effective masked diffusion language
662 models. *arXiv preprint arXiv:2406.07524*, 2024a.
- 664 Subham Sekhar Sahoo, Aaron Gokaslan, Chris De Sa, and Volodymyr Kuleshov. Diffusion models
665 with learned adaptive noise. *arXiv preprint arXiv:2312.13236*, 2024b.
- 666 Tim Salimans, Ian Goodfellow, Wojciech Zaremba, Vicki Cheung, Alec Radford, and Xi Chen.
667 Improved techniques for training gans. *Advances in neural information processing systems*, 29,
668 2016.
- 669 Guillaume Sanchez, Honglu Fan, Alexander Spangher, Elad Levi, Pawan Sasanka Ammanamanchi,
670 and Stella Biderman. Stay on topic with classifier-free guidance. *arXiv preprint*
671 *arXiv:2306.17806*, 2023.
- 673 Anirban Sarkar, Ziqi Tang, Chris Zhao, and Peter Koo. Designing dna with tunable regulatory
674 activity using discrete diffusion. *bioRxiv*, pp. 2024–05, 2024.
- 675 Yair Schiff, Chia-Hsiang Kao, Aaron Gokaslan, Tri Dao, Albert Gu, and Volodymyr Kuleshov.
676 Caduceus: Bi-directional equivariant long-range dna sequence modeling. *arXiv preprint*
677 *arXiv:2403.03234*, 2024.
- 679 Philippe Schwaller, Teodoro Laino, Théophile Gaudin, Peter Bolgar, Christopher A Hunter, Costas
680 Bekas, and Alpha A Lee. Molecular transformer: A model for uncertainty-calibrated chemical
681 reaction prediction. *ACS central science*, 5(9):1572–1583, 2019.
- 682 Jiaxin Shi, Kehang Han, Zhe Wang, Arnaud Doucet, and Michalis K Titsias. Simplified and gener-
683 alized masked diffusion for discrete data. *arXiv preprint arXiv:2406.04329*, 2024.
- 684 Jascha Sohl-Dickstein, Eric Weiss, Niru Maheswaranathan, and Surya Ganguli. Deep unsupervised
685 learning using nonequilibrium thermodynamics. In *International conference on machine learn-*
686 *ing*, pp. 2256–2265. PMLR, 2015.
- 688 Yang Song and Stefano Ermon. Generative modeling by estimating gradients of the data distribution.
689 *Advances in neural information processing systems*, 32, 2019.
- 690 Jianlin Su, Yu Lu, Shengfeng Pan, Ahmed Murtadha, Bo Wen, and Yunfeng Liu. Roformer: En-
691 hanced transformer with rotary position embedding. *arXiv preprint arXiv:2104.09864*, 2021.
- 693 Haoran Sun, Lijun Yu, Bo Dai, Dale Schuurmans, and Hanjun Dai. Score-based continuous-time
694 discrete diffusion models. *arXiv preprint arXiv:2211.16750*, 2022.
- 695 Clement Vignac, Igor Krawczuk, Antoine Siraudin, Bohan Wang, Volkan Cevher, and Pas-
696 cal Frossard. Digress: Discrete denoising diffusion for graph generation. *arXiv preprint*
697 *arXiv:2209.14734*, 2022.
- 699 Yingheng Wang, Yair Schiff, Aaron Gokaslan, Weishen Pan, Fei Wang, Christopher De Sa, and
700 Volodymyr Kuleshov. Infodiffusion: Representation learning using information maximizing dif-
701 fusion models. In *International Conference on Machine Learning*, pp. 36336–36354. PMLR,
2023.

- 702 David Weininger. Smiles, a chemical language and information system. 1. introduction to method-
703 ology and encoding rules. *Journal of chemical information and computer sciences*, 28(1):31–36,
704 1988.
- 705
706 Thomas Wolf, Lysandre Debut, Victor Sanh, Julien Chaumond, Clement Delangue, Anthony Moi,
707 Pierric Cistac, Tim Rault, Rémi Louf, Morgan Funtowicz, Joe Davison, Sam Shleifer, Patrick
708 von Platen, Clara Ma, Yacine Jernite, Julien Plu, Canwen Xu, Teven Le Scao, Sylvain Gug-
709 ger, Mariama Drame, Quentin Lhoest, and Alexander M. Rush. Transformers: State-of-the-art
710 natural language processing. In *Proceedings of the 2020 Conference on Empirical Methods in*
711 *Natural Language Processing: System Demonstrations*, pp. 38–45, Online, October 2020. As-
712 sociation for Computational Linguistics. URL [https://www.aclweb.org/anthology/
2020.emnlp-demos.6](https://www.aclweb.org/anthology/2020.emnlp-demos.6).
- 713
714 Kevin Yang and Dan Klein. Fudge: Controlled text generation with future discriminators. *arXiv*
715 *preprint arXiv:2104.05218*, 2021.
- 716
717 Xiang Zhang, Junbo Zhao, and Yann LeCun. Character-level convolutional networks for text clas-
718 sification. *Advances in neural information processing systems*, 28, 2015.
- 719
720 Lingxiao Zhao, Xueying Ding, Lijun Yu, and Leman Akoglu. Improving and unifying
721 discrete&continuous-time discrete denoising diffusion. *arXiv preprint arXiv:2402.03701*, 2024.
- 722
723 Lin Zheng, Jianbo Yuan, Lei Yu, and Lingpeng Kong. A reparameterized discrete diffusion model
724 for text generation. *arXiv preprint arXiv:2302.05737*, 2023.
- 725
726
727
728
729
730
731
732
733
734
735
736
737
738
739
740
741
742
743
744
745
746
747
748
749
750
751
752
753
754
755

A CONTINUOUS TIME DISCRETE UNIFORM DIFFUSION

Here, we derive a continuous time formulation ($T \rightarrow \infty$) for the diffusion loss term $\mathcal{L}_{\text{diffusion}}$ when using the uniform distribution as the limiting distribution of the diffusion process.

For uniform noise diffusion, we define a limiting distribution $\mathbf{u} = \mathbf{1}/N$, where $\mathbf{1}$ represents the column vector of all ones, and N the size of the vocabulary. We adopt the assumption from MDLM (Sahoo et al., 2024a) that our diffusion process interpolates between clean data and noise:

$$q(\mathbf{z}_t | \mathbf{x}) = \text{Cat}(\mathbf{z}_t; \alpha_t \mathbf{x} + (1 - \alpha_t) \boldsymbol{\pi}) \quad (15)$$

and the marginals are given as

$$q(\mathbf{z}_t | \mathbf{z}_s) = \text{Cat}(\mathbf{z}_t; \alpha_{t|s} \mathbf{z}_s + (1 - \alpha_{t|s}) \boldsymbol{\pi}), \quad (16)$$

where $\alpha_{t|s} = \alpha_t / \alpha_s$.

Following Austin et al. (2021), we can derive the posterior:

$$q(\mathbf{z}_s | \mathbf{z}_t, \mathbf{x}) = \text{Cat} \left(\mathbf{z}_s; \frac{[\alpha_{t|s} \mathbf{z}_t + (1 - \alpha_{t|s}) \mathbf{1} \boldsymbol{\pi}^\top \mathbf{z}_t] \odot [\alpha_s \mathbf{x} + (1 - \alpha_s) \boldsymbol{\pi}]}{\alpha_t \langle \mathbf{z}_t, \mathbf{x} \rangle + (1 - \alpha_t) \mathbf{z}_t^\top \boldsymbol{\pi}} \right). \quad (17)$$

Using $\boldsymbol{\pi} = \mathbf{u}$ as defined above, we get the following:

$$q(\mathbf{z}_s | \mathbf{z}_t, \mathbf{x}) = \text{Cat} \left(\mathbf{z}_s; \frac{\alpha_t \mathbf{z}_t \odot \mathbf{x} + \frac{(\alpha_{t|s} - \alpha_t)}{N} \mathbf{z}_t + \frac{(\alpha_s - \alpha_t)}{N} \mathbf{x} + \frac{(1 - \alpha_{t|s})(1 - \alpha_s)}{N^2} \mathbf{1}}{\alpha_t \langle \mathbf{z}_t, \mathbf{x} \rangle + \frac{(1 - \alpha_t)}{N}} \right) \quad (18)$$

$$= \text{Cat} \left(\mathbf{z}_s; \frac{N \alpha_t \mathbf{z}_t \odot \mathbf{x} + (\alpha_{t|s} - \alpha_t) \mathbf{z}_t + (\alpha_s - \alpha_t) \mathbf{x} + \frac{(\alpha_s - \alpha_t)(1 - \alpha_s)}{N \alpha_s} \mathbf{1}}{N \alpha_t \langle \mathbf{z}_t, \mathbf{x} \rangle + 1 - \alpha_t} \right). \quad (19)$$

For the denoising distribution, we replace \mathbf{x} by \mathbf{x}_θ :

$$p_\theta(\mathbf{z}_s | \mathbf{z}_t) = \text{Cat} \left(\mathbf{z}_s; \frac{N \alpha_t \mathbf{z}_t \odot \mathbf{x}_\theta + (\alpha_{t|s} - \alpha_t) \mathbf{z}_t + (\alpha_s - \alpha_t) \mathbf{x}_\theta + \frac{(\alpha_s - \alpha_t)(1 - \alpha_s)}{\alpha_s N} \mathbf{1}}{N \alpha_t \langle \mathbf{z}_t, \mathbf{x}_\theta \rangle + 1 - \alpha_t} \right). \quad (20)$$

Let us now look at the diffusion loss term in the NELBO:

$$T \cdot D_{\text{KL}}(q(\mathbf{z}_s | \mathbf{z}_t, \mathbf{x}) || p_\theta(\mathbf{z}_s | \mathbf{z}_t)) = T \cdot \sum_{j \in [N]} q(\mathbf{z}_s | \mathbf{z}_t, \mathbf{x})_j \log \left(\frac{q(\mathbf{z}_s | \mathbf{z}_t, \mathbf{x})_j}{p_\theta(\mathbf{z}_s | \mathbf{z}_t)_j} \right). \quad (21)$$

Letting $i = \arg \max_{j \in [N]} (\mathbf{z}_t)_j$ be the non-zero entry of \mathbf{z}_t , we can break up this KL into two terms:

$$\begin{aligned} T \cdot D_{\text{KL}}(q(\mathbf{z}_s | \mathbf{z}_t, \mathbf{x}) || p_\theta(\mathbf{z}_s | \mathbf{z}_t)) &= T \cdot \underbrace{q(\mathbf{z}_s | \mathbf{z}_t, \mathbf{x})_i \log \left(\frac{q(\mathbf{z}_s | \mathbf{z}_t, \mathbf{x})_i}{p_\theta(\mathbf{z}_s | \mathbf{z}_t)_i} \right)}_{\text{Term 1}} \\ &\quad + T \cdot \underbrace{\sum_{\substack{j \in [N] \\ \text{s.t. } (\mathbf{z}_t)_j = 0}} q(\mathbf{z}_s | \mathbf{z}_t, \mathbf{x})_j \log \left(\frac{q(\mathbf{z}_s | \mathbf{z}_t, \mathbf{x})_j}{p_\theta(\mathbf{z}_s | \mathbf{z}_t)_j} \right)}_{\text{Term 2}}. \end{aligned} \quad (22)$$

We now examine each of these terms taking $T \rightarrow \infty$, or equivalently, using $s = t - \frac{1}{T} \implies T = \frac{1}{t-s}$, taking $s \rightarrow t$.

Term 1:

$$\begin{aligned} \lim_{s \rightarrow t} \frac{1}{t-s} \cdot \frac{N \alpha_t \mathbf{x}_i + \alpha_{t|s} - \alpha_t + (\alpha_s - \alpha_t) \mathbf{x}_i + \frac{(\alpha_s - \alpha_t)(1 - \alpha_s)}{\alpha_s N}}{N \alpha_t \mathbf{x}_i + 1 - \alpha_t} \\ \cdot \log \left[\frac{\frac{N \alpha_t \mathbf{x}_i + \alpha_{t|s} - \alpha_t + (\alpha_s - \alpha_t) \mathbf{x}_i + \frac{(\alpha_s - \alpha_t)(1 - \alpha_s)}{\alpha_s N}}{N \alpha_t \mathbf{x}_i + 1 - \alpha_t}}{\frac{N \alpha_t (\mathbf{x}_\theta)_i + \alpha_{t|s} - \alpha_t + (\alpha_s - \alpha_t) (\mathbf{x}_\theta)_i + \frac{(\alpha_s - \alpha_t)(1 - \alpha_s)}{\alpha_s N}}{N \alpha_t (\mathbf{x}_\theta)_i + 1 - \alpha_t}} \right] \end{aligned} \quad (23)$$

As $s \rightarrow t$, the coefficient on the log term will approach 1. Additionally both the numerator and the denominator inside the log term will approach 1, thus the entire log term will approach 0. Combining this with the fact that $t - s$ will approach 0, gives us the indeterminate form of $0/0$, hence we apply L'Hôpital's rule to (23). Writing q and p_θ as functions of s , when we differentiate the log term we get:

$$\begin{aligned} \frac{d}{ds} \log \left[\frac{q(s)}{p_\theta(s)} \right] &= \frac{d}{ds} \log q(s) - \frac{d}{ds} \log p_\theta(s) \\ &= \frac{\frac{d}{ds} q(s)}{q(s)} - \frac{\frac{d}{ds} p_\theta(s)}{p_\theta(s)} \end{aligned} \quad (24)$$

Let's look at each derivative term in (24):

$$\begin{aligned} \lim_{s \rightarrow t} \frac{d}{ds} q(s) &= \lim_{s \rightarrow t} \frac{\frac{-\alpha'_s \alpha_t}{\alpha_s^2} + \alpha'_s (\mathbf{x}_\theta)_i + \frac{N \alpha_s [\alpha'_s (1 - \alpha_s) - \alpha'_s (\alpha_s - \alpha_t)] - [N \alpha'_s (\alpha_s - \alpha_t) (1 - \alpha_s)]}{N \alpha_s^2}}{N \alpha_t \mathbf{x}_i + 1 - \alpha_t} \\ &= \frac{\frac{-\alpha'_t}{\alpha_t} + \alpha'_t \mathbf{x}_i + \frac{\alpha'_t (1 - \alpha_t)}{N \alpha_t}}{N \alpha_t \mathbf{x}_i + 1 - \alpha_t} \\ &= \frac{\alpha'_t}{N \alpha_t} \left[\frac{-N + N \alpha_t \mathbf{x}_i + 1 - \alpha_t}{N \alpha_t \mathbf{x}_i + 1 - \alpha_t} \right] \\ &= \frac{\alpha'_t}{N \alpha_t} \left[1 - \frac{N}{N \alpha_t \mathbf{x}_i + 1 - \alpha_t} \right] \end{aligned} \quad (25)$$

Similarly,

$$\lim_{s \rightarrow t} \frac{d}{ds} p_\theta(s) = \frac{\alpha'_t}{N \alpha_t} \left[1 - \frac{N}{N \alpha_t (\mathbf{x}_\theta)_i + 1 - \alpha_t} \right] \quad (26)$$

Note that when taking $s \rightarrow t$, both $q(s)$ and $p_\theta(s)$ evaluate to 1. Additionally, differentiating $\frac{1}{t-s}$ with respect to s evaluates to -1 . When combining these facts and plugging (25) and (26) into (24), (23) becomes

$$\begin{aligned} \lim_{s \rightarrow t} \text{Term 1} &= \frac{-\alpha'_t}{N \alpha_t} \left[1 - \frac{N}{N \alpha_t \mathbf{x}_i + 1 - \alpha_t} \right] + \frac{\alpha'_t}{N \alpha_t} \left[1 - \frac{N}{N \alpha_t (\mathbf{x}_\theta)_i + 1 - \alpha_t} \right] \\ &= \frac{\alpha'_t}{N \alpha_t} \left[\frac{N}{N \alpha_t \mathbf{x}_i + 1 - \alpha_t} - \frac{N}{N \alpha_t (\mathbf{x}_\theta)_i + 1 - \alpha_t} \right] \end{aligned} \quad (27)$$

Term 2:

$$\lim_{s \rightarrow t} \frac{1}{t-s} \cdot \sum_{\substack{j \in [N] \\ \text{s.t. } (\mathbf{z}_t)_j = 0}} \frac{(\alpha_s - \alpha_t) \mathbf{x}_j + \frac{(\alpha_s - \alpha_t)(1 - \alpha_s)}{N \alpha_s}}{N \alpha_t \mathbf{x}_i + 1 - \alpha_t} \log \left[\frac{\frac{(\alpha_s - \alpha_t) \mathbf{x}_j + \frac{(\alpha_s - \alpha_t)(1 - \alpha_s)}{N \alpha_s}}{N \alpha_t \mathbf{x}_i + 1 - \alpha_t}}{\frac{(\alpha_s - \alpha_t) (\mathbf{x}_\theta)_j + \frac{(\alpha_s - \alpha_t)(1 - \alpha_t)}{N \alpha_s}}{N \alpha_t (\mathbf{x}_\theta)_i + 1 - \alpha_t}} \right] \quad (28)$$

For each term in the summation, $\frac{1}{t-s}$ times the coefficient on the log term will have an indeterminate form of $0/0$ as $s \rightarrow t$. We therefore apply L'Hôpital's rule to this coefficient:

$$\lim_{s \rightarrow t} \frac{1}{t-s} \cdot \frac{(\alpha_s - \alpha_t) \mathbf{x}_j + \frac{(\alpha_s - \alpha_t)(1 - \alpha_s)}{N \alpha_s}}{N \alpha_t \mathbf{x}_i + 1 - \alpha_t} = \frac{-\alpha'_t}{N \alpha_t} \left[\frac{N \alpha_t \mathbf{x}_j + 1 - \alpha_t}{N \alpha_t \mathbf{x}_i + 1 - \alpha_t} \right] \quad (29)$$

Now, for the log term, we exchange the limit with the continuous log function and have that both the numerator and the denominator go to zero as $s \rightarrow t$. We therefore apply L'Hôpital's rule here as

well:

$$\begin{aligned}
& \log \lim_{s \rightarrow t} \left[\frac{(\alpha_s - \alpha_t) \mathbf{x}_j + \frac{(\alpha_s - \alpha_t)(1 - \alpha_s)}{N \alpha_s}}{N \alpha_t \mathbf{x}_i + 1 - \alpha_t} \right] = \log \lim_{s \rightarrow t} \left[\frac{\frac{d}{ds} (\alpha_s - \alpha_t) \mathbf{x}_j + \frac{(\alpha_s - \alpha_t)(1 - \alpha_s)}{N \alpha_s}}{N \alpha_t \mathbf{x}_i + 1 - \alpha_t} \right] \\
& \left[\frac{(\alpha_s - \alpha_t)(\mathbf{x}_\theta)_j + \frac{(\alpha_s - \alpha_t)(1 - \alpha_t)}{N \alpha_s}}{N \alpha_t (\mathbf{x}_\theta)_i + 1 - \alpha_t} \right] \\
& = \log \left[\left(\frac{N \alpha_t (\mathbf{x}_\theta)_i + 1 - \alpha_t}{N \alpha_t \mathbf{x}_i + 1 - \alpha_t} \right) \left(\frac{\alpha'_t \mathbf{x}_j + \frac{\alpha'_t (1 - \alpha_t)}{N \alpha_t}}{\alpha'_t (\mathbf{x}_\theta)_j + \frac{\alpha'_t (1 - \alpha_t)}{N \alpha_t}} \right) \right] \\
& = \log \left[\left(\frac{N \alpha_t (\mathbf{x}_\theta)_i + 1 - \alpha_t}{N \alpha_t \mathbf{x}_i + 1 - \alpha_t} \right) \left(\frac{\frac{\alpha'_t}{N \alpha_t} (N \alpha_t \mathbf{x}_j + 1 - \alpha_t)}{\frac{\alpha'_t}{N \alpha_t} (N \alpha_t (\mathbf{x}_\theta)_j + 1 - \alpha_t)} \right) \right] \\
& = \log \left[\left(\frac{N \alpha_t (\mathbf{x}_\theta)_i + 1 - \alpha_t}{N \alpha_t \mathbf{x}_i + 1 - \alpha_t} \right) \left(\frac{N \alpha_t \mathbf{x}_j + 1 - \alpha_t}{N \alpha_t (\mathbf{x}_\theta)_j + 1 - \alpha_t} \right) \right] \\
& = \log \left[\left(\frac{N \alpha_t (\mathbf{x}_\theta)_i + 1 - \alpha_t}{N \alpha_t (\mathbf{x}_\theta)_j + 1 - \alpha_t} \right) \left(\frac{N \alpha_t \mathbf{x}_j + 1 - \alpha_t}{N \alpha_t \mathbf{x}_i + 1 - \alpha_t} \right) \right] \tag{30}
\end{aligned}$$

Multiplying (29) by (30), we get:

$$\lim_{s \rightarrow t} \text{Term 2} = \frac{-\alpha'_t}{N \alpha_t} \sum_{\substack{j \in [N] \\ \text{s.t. } (\mathbf{z}_t)_j = 0}} \left(\frac{N \alpha_t \mathbf{x}_j + 1 - \alpha_t}{N \alpha_t \mathbf{x}_i + 1 - \alpha_t} \right) \log \left[\left(\frac{N \alpha_t (\mathbf{x}_\theta)_i + 1 - \alpha_t}{N \alpha_t (\mathbf{x}_\theta)_j + 1 - \alpha_t} \right) \left(\frac{N \alpha_t \mathbf{x}_j + 1 - \alpha_t}{N \alpha_t \mathbf{x}_i + 1 - \alpha_t} \right) \right] \tag{31}$$

Combining Terms 1 and 2: Using (27) and (31), the final KL term in the continuous time limit is:

$$\begin{aligned}
\lim_{T \rightarrow \infty} T \cdot D_{\text{KL}}(q || p_\theta) &= \frac{\alpha'_t}{N \alpha_t} \left[\frac{N}{N \alpha_t \mathbf{x}_i + 1 - \alpha_t} - \frac{N}{N \alpha_t (\mathbf{x}_\theta)_i + 1 - \alpha_t} \right. \\
&\quad \left. - \sum_{\substack{j \in [N] \\ \text{s.t. } (\mathbf{z}_t)_j = 0}} \left(\frac{N \alpha_t \mathbf{x}_j + 1 - \alpha_t}{N \alpha_t \mathbf{x}_i + 1 - \alpha_t} \right) \log \left[\left(\frac{N \alpha_t (\mathbf{x}_\theta)_i + 1 - \alpha_t}{N \alpha_t (\mathbf{x}_\theta)_j + 1 - \alpha_t} \right) \left(\frac{N \alpha_t \mathbf{x}_j + 1 - \alpha_t}{N \alpha_t \mathbf{x}_i + 1 - \alpha_t} \right) \right] \right].
\end{aligned}$$

Defining $\bar{\mathbf{x}} = N \alpha_t \mathbf{x} + (1 - \alpha_t) \mathbf{1}$ and $\bar{\mathbf{x}}_\theta = N \alpha_t \mathbf{x}_\theta + (1 - \alpha_t) \mathbf{1}$, as in Section 4.2, yields the desired result.

B RELATING UDLM TO CTMC

Similar to Sahoo et al. (2024a), our work tackles the problem of discrete diffusion from the variational perspective and analyzes the ELBO in the continuous time limit. In contrast, other works, such as Campbell et al. (2022) and Lou et al. (2023), have extended the discrete diffusion framework proposed in Austin et al. (2021) using the formalisms of continuous time Markov chains (CTMC). In this section, we relate these two approaches.

Background on CTMC In the CTMC formulation, the key quantity of interest is the **rate matrix** $R_t \in \mathbb{R}^{N \times N}$. In analogy to the discrete time transition matrices Q_t , which define the transition probabilities between states, these rate matrices define the instantaneous rate of change between states in continuous time. More formally, letting δ be the Kronecker delta function, and using \mathbf{z} and \mathbf{z}' to denote observed values of the latents, we can define the forward noising process using R_t as follows:

$$q(\mathbf{z}_t = \mathbf{z}' \mid \mathbf{z}_s = \mathbf{z}) = \delta_{\mathbf{z}', \mathbf{z}} + R_t(\mathbf{z}, \mathbf{z}') \frac{1}{T} + o\left(\frac{1}{T}\right) \tag{32}$$

where $o(1/T)$ indicates terms that vanish more quickly than $1/T$. Recall that we defined $s = t - \frac{1}{T}$. In continuous time, as $T \rightarrow \infty$, $o(1/T)$ terms are ignored, and we have

$$R_t(\mathbf{z}, \mathbf{z}') = \lim_{T \rightarrow \infty} \frac{q(\mathbf{z}_t = \mathbf{z}' \mid \mathbf{z}_{t-(1/T)} = \mathbf{z}) - \delta_{\mathbf{z}', \mathbf{z}}}{1/T}, \tag{33}$$

918 hence our treatment of R_t as the ‘instantaneous’ rate of state transitions.

919 Importantly, processes defined as in (32) have known time reversal processes given by (Kelly, 2011;
920 Sun et al., 2022):

$$921 \quad q(\mathbf{z}_s = \mathbf{z}' \mid \mathbf{z}_t = \mathbf{z}) = \delta_{\mathbf{z}', \mathbf{z}} + \check{R}_t(\mathbf{z}, \mathbf{z}') \frac{1}{T} + o\left(\frac{1}{T}\right), \quad (34)$$

922 where \check{R}_t represents the reverse rate matrix which is related to the forward matrix as follows:

$$923 \quad \check{R}_t(\mathbf{z}', \mathbf{z}) = \frac{q(\mathbf{z}_t = \mathbf{z}')}{q(\mathbf{z}_t = \mathbf{z})} R_t(\mathbf{z}, \mathbf{z}'), \quad \text{if } \mathbf{z}' \neq \mathbf{z} \quad (35)$$

924 with $\check{R}_t(\mathbf{z}, \mathbf{z}) = -\sum_{\mathbf{z}' \neq \mathbf{z}} \check{R}_t(\mathbf{z}', \mathbf{z})$, which ensures that the rows of \check{R}_t sum to zero (i.e., mass cannot
925 be created or destroyed). Note that in (35), we are scaling the forward rate matrix by a ratio of the
926 unconditional marginals: $q(\mathbf{z}_t = \mathbf{z}')/q(\mathbf{z}_t = \mathbf{z})$.

927 **Forward Rate Matrices for Uniform Noise** Recall from the analysis in Appendix A that we can
928 use L’Hospital’s rule to evaluate $\lim_{T \rightarrow \infty} T \cdot (1 - \alpha_{t|s}) = -\alpha'_t/\alpha_t$. Now, using (16) from above,
929 for $\mathbf{z}' \neq \mathbf{z}$ we have

$$930 \quad q(\mathbf{z}_t = \mathbf{z}' \mid \mathbf{z}_s = \mathbf{z}) = \frac{1 - \alpha_{t|s}}{N}. \quad (36)$$

931 Combining this with (33), we have that:

$$932 \quad R_t(\mathbf{z}, \mathbf{z}') = \lim_{T \rightarrow \infty} T \cdot \frac{1 - \alpha_{t|s}}{N} = -\frac{\alpha'_t}{N\alpha_t}. \quad (37)$$

933 Now for $\mathbf{z}' = \mathbf{z}$, again from (16), we have

$$934 \quad q(\mathbf{z}_t = \mathbf{z} \mid \mathbf{z}_s = \mathbf{z}) = \alpha_{t|s} + \frac{1 - \alpha_{t|s}}{N}, \quad (38)$$

935 which combines with (33) to yield:

$$936 \quad R_t(\mathbf{z}, \mathbf{z}) = \lim_{T \rightarrow \infty} T \cdot \left(\alpha_{t|s} + \frac{1 - \alpha_{t|s}}{N} - 1 \right) = \frac{1 - N}{N} \lim_{T \rightarrow \infty} T \cdot (1 - \alpha_{t|s}) = \frac{-\alpha'_t}{N\alpha_t} (1 - N). \quad (39)$$

937 Writing (37) and (39) as a single expression, gives:

$$938 \quad R_t(\mathbf{z}, \mathbf{z}') = -\frac{\alpha'_t}{N\alpha_t} [\mathbf{1}\mathbf{1}^\top - N\mathbf{I}]. \quad (40)$$

939 B.1 EQUIVALENCE OF UDLM ELBO AND SEDD ELBO

940 Below, we demonstrate that the variational lower bound from (13) used to train UDLM is equivalent
941 to the lower bound derived in SEDD (Lou et al., 2023).

942 **Notation** To facilitate the discussion, we introduce a notational shorthand $q_t(\mathbf{z}') = q(\mathbf{z}_t = \mathbf{z}')$
943 and $q_t(\mathbf{z}' \mid \mathbf{x}) = q(\mathbf{z}_t = \mathbf{z}' \mid \mathbf{x})$.

944 In SEDD, the quantity of interest is the ratio of probabilities in the reverse rate matrix equation given
945 in (35), and they train a parametric model to learn this so-called concrete score (Meng et al., 2022):

$$946 \quad s_\theta(\mathbf{z})_{\mathbf{z}'} \approx \frac{q_t(\mathbf{z}')}{q_t(\mathbf{z})}. \quad (41)$$

947 Since the unconditional marginals in this ratio are intractable, SEDD proposes a tractable denoising
948 score-based objective. Importantly, they show that the denoising score-based objective they use
949 for training serves as variational bound and derive the following expression for Negative Evidence
950 Lower Bound (NELBO):

$$951 \quad \text{NELBO}_{\text{SEDD}} \\ 952 \quad = \mathbb{E}_{t \in [0, 1], \mathbf{z} \sim q_t(\cdot | \mathbf{x})} \left[\sum_{\mathbf{z}' \neq \mathbf{z}_t} R_t(\mathbf{z}, \mathbf{z}') \left(s_\theta(\mathbf{z})_{\mathbf{z}'} - \frac{q_t(\mathbf{z}' | \mathbf{x})}{q_t(\mathbf{z} | \mathbf{x})} \log s_\theta(\mathbf{z})_{\mathbf{z}'} + K \left(\frac{q_t(\mathbf{z}' | \mathbf{x})}{q_t(\mathbf{z} | \mathbf{x})} \right) \right) \right], \quad (42)$$

953 where $K(a) = a(\log a - 1)$ for $a \in \mathbb{R}^+$.

SEDD with Interpolating Uniform Noise From (1) we have $q_t(\mathbf{z}|\mathbf{x}) = \alpha_t \mathbf{x}_i + (1 - \alpha_t)/N$ where i is the non-zero index of the one-hot vector \mathbf{z} , i.e., $\mathbf{z}_i = 1$. Thus, the “true” conditional score in (42) can be written as

$$\frac{q_t(\mathbf{z}'|\mathbf{x})}{q_t(\mathbf{z}|\mathbf{x})} = \frac{\alpha_t \mathbf{x}_j + (1 - \alpha_t)/N}{\alpha_t \mathbf{x}_i + (1 - \alpha_t)/N} = \frac{N\alpha_t \mathbf{x}_j + (1 - \alpha_t)}{N\alpha_t \mathbf{x}_i + (1 - \alpha_t)}, \quad (43)$$

where again we use i and j to denote the non-zero indices of the one-hot vectors \mathbf{z} and \mathbf{z}' , respectively.

Using Mean Parameterization in SEDD NELBO In our work, we use the mean parameterization, that is we predict the ‘clean’ data given noisy observations using the model that we denote as \mathbf{x}_θ . Note that (42) is minimized if

$$\mathbf{s}_\theta(\mathbf{z})_{\mathbf{z}'} = \frac{q_t(\mathbf{z}'|\mathbf{x})}{q_t(\mathbf{z}|\mathbf{x})}.$$

Thus, we can replace \mathbf{x} in (43) to extract a score model from our parameterization:

$$\mathbf{s}_\theta(\mathbf{z})_{\mathbf{z}'} = \frac{\alpha_t (\mathbf{x}_\theta)_j + (1 - \alpha_t)/N}{\alpha_t (\mathbf{x}_\theta)_i + (1 - \alpha_t)/N} = \frac{N\alpha_t (\mathbf{x}_\theta)_j + (1 - \alpha_t)}{N\alpha_t (\mathbf{x}_\theta)_i + (1 - \alpha_t)}. \quad (44)$$

We now show two useful identities that come from this parameterization. First,

$$\begin{aligned} \sum_{\mathbf{z}' \neq \mathbf{z}} \mathbf{s}_\theta(\mathbf{z})_{\mathbf{z}'} &= \sum_{j \neq i} \frac{\alpha_t (\mathbf{x}_\theta)_j + (1 - \alpha_t)/N}{\alpha_t (\mathbf{x}_\theta)_i + (1 - \alpha_t)/N} \\ &= \frac{\alpha_t [\sum_{j \neq i} (\mathbf{x}_\theta)_j] + \sum_{j \neq i} (1 - \alpha_t)/N}{\alpha_t (\mathbf{x}_\theta)_i + (1 - \alpha_t)/N} \\ &= \frac{\alpha_t [\sum_{j \neq i} (\mathbf{x}_\theta)_j] + (1 - \alpha_t)(N - 1)/N}{\alpha_t (\mathbf{x}_\theta)_i + (1 - \alpha_t)/N} && \because \sum_{j=1}^N 1 = N \implies \sum_{j \neq i} 1 = N - 1 \\ &= \frac{\alpha_t [1 - (\mathbf{x}_\theta)_i] + (1 - \alpha_t) - (1 - \alpha_t)/N}{\alpha_t (\mathbf{x}_\theta)_i + (1 - \alpha_t)/N} && \because \sum_j (\mathbf{x}_\theta)_j = 1 \implies \sum_{j \neq i} (\mathbf{x}_\theta)_j = 1 - (\mathbf{x}_\theta)_i \\ &= \frac{\alpha_t + (1 - \alpha_t) - \alpha_t (\mathbf{x}_\theta)_i - (1 - \alpha_t)/N}{\alpha_t (\mathbf{x}_\theta)_i + (1 - \alpha_t)/N} \\ &= \frac{1 - \alpha_t (\mathbf{x}_\theta)_i - (1 - \alpha_t)/N}{\alpha_t (\mathbf{x}_\theta)_i + (1 - \alpha_t)/N} \\ &= \frac{1}{\alpha_t (\mathbf{x}_\theta)_i + (1 - \alpha_t)/N} - 1 \\ &= \frac{N}{N\alpha_t (\mathbf{x}_\theta)_i + (1 - \alpha_t)} - 1 \end{aligned} \quad (45)$$

The same logic can be applied to show that

$$\sum_{\mathbf{z}' \neq \mathbf{z}} \frac{q_t(\mathbf{z}'|\mathbf{x})}{q_t(\mathbf{z}|\mathbf{x})} = \sum_{j \neq i} \frac{\alpha_t \mathbf{x}_j + (1 - \alpha_t)/N}{\alpha_t \mathbf{x}_i + (1 - \alpha_t)/N} = \frac{N}{N\alpha_t \mathbf{x}_i + (1 - \alpha_t)} - 1. \quad (46)$$

Equivalence Between NELBO_{SEDD} and NELBO_{UDLM} We can now use the identities from (45) and (46) to demonstrate that NELBO_{SEDD} (42) is equivalent to NELBO_{UDLM} (13).

NELBO_{SEDD}

$$\begin{aligned}
&= \mathbb{E}_{t \in [0,1], \mathbf{z} \sim q_t(\cdot|\mathbf{x})} \left[\sum_{\mathbf{z}' \neq \mathbf{z}} R_t(\mathbf{z}, \mathbf{z}') \left(\mathbf{s}_\theta(\mathbf{z})_{\mathbf{z}'} - \frac{q_t(\mathbf{z}'|\mathbf{x})}{q_t(\mathbf{z}|\mathbf{x})} \log \mathbf{s}_\theta(\mathbf{z})_{\mathbf{z}'} + K \left(\frac{q_t(\mathbf{z}'|\mathbf{x})}{q_t(\mathbf{z}|\mathbf{x})} \right) \right) \right] \\
&= \mathbb{E}_{t \in [0,1], \mathbf{z} \sim q_t(\cdot|\mathbf{x})} \left[\sum_{\mathbf{z}' \neq \mathbf{z}} -\frac{\alpha'_t}{N\alpha_t} \left(\mathbf{s}_\theta(\mathbf{z})_{\mathbf{z}'} - \frac{q_t(\mathbf{z}'|\mathbf{x})}{q_t(\mathbf{z}|\mathbf{x})} \log \mathbf{s}_\theta(\mathbf{z})_{\mathbf{z}'} + K \left(\frac{q_t(\mathbf{z}'|\mathbf{x})}{q_t(\mathbf{z}|\mathbf{x})} \right) \right) \right] \quad \text{from (37)} \\
&= \mathbb{E}_{t \in [0,1], \mathbf{z} \sim q_t(\cdot|\mathbf{x})} \left[\frac{\alpha'_t}{N\alpha_t} \left(-\sum_{\mathbf{z}' \neq \mathbf{z}} \mathbf{s}_\theta(\mathbf{z})_{\mathbf{z}'} + \sum_{\mathbf{z}' \neq \mathbf{z}} \frac{q_t(\mathbf{z}'|\mathbf{x})}{q_t(\mathbf{z}|\mathbf{x})} \log \mathbf{s}_\theta(\mathbf{z})_{\mathbf{z}'} - \sum_{\mathbf{z}' \neq \mathbf{z}} K \left(\frac{q_t(\mathbf{z}'|\mathbf{x})}{q_t(\mathbf{z}|\mathbf{x})} \right) \right) \right]
\end{aligned}$$

Recall that $K(a) = a \log a - a$

$$= \mathbb{E}_{t \in [0,1], \mathbf{z} \sim q_t(\cdot|\mathbf{x})} \frac{\alpha'_t}{N\alpha_t} \left[-\sum_{\mathbf{z}' \neq \mathbf{z}} \mathbf{s}_\theta(\mathbf{z})_{\mathbf{z}'} + \sum_{\mathbf{z}' \neq \mathbf{z}} \frac{q_t(\mathbf{z}'|\mathbf{x})}{q_t(\mathbf{z}|\mathbf{x})} \log \mathbf{s}_\theta(\mathbf{z})_{\mathbf{z}'} - \sum_{\mathbf{z}' \neq \mathbf{z}} \frac{q_t(\mathbf{z}'|\mathbf{x})}{q_t(\mathbf{z}|\mathbf{x})} \log \frac{q_t(\mathbf{z}'|\mathbf{x})}{q_t(\mathbf{z}|\mathbf{x})} + \sum_{\mathbf{z}' \neq \mathbf{z}} \frac{q_t(\mathbf{z}'|\mathbf{x})}{q_t(\mathbf{z}|\mathbf{x})} \right]$$

Using (45) and (46) we get,

$$\begin{aligned}
&= \mathbb{E}_{t \in [0,1], \mathbf{z} \sim q_t(\cdot|\mathbf{x})} \frac{\alpha'_t}{N\alpha_t} \left[-\frac{N}{\alpha_t N(\mathbf{x}_\theta)_i + (1 - \alpha_t)} + \frac{N}{\alpha_t N\mathbf{x}_i + (1 - \alpha_t)} \right. \\
&\quad \left. + \sum_{\mathbf{z}' \neq \mathbf{z}} \frac{q_t(\mathbf{z}'|\mathbf{x})}{q_t(\mathbf{z}|\mathbf{x})} \log \mathbf{s}_\theta(\mathbf{z})_{\mathbf{z}'} - \sum_{\mathbf{z}' \neq \mathbf{z}} \frac{q_t(\mathbf{z}'|\mathbf{x})}{q_t(\mathbf{z}|\mathbf{x})} \log \frac{q_t(\mathbf{z}'|\mathbf{x})}{q_t(\mathbf{z}|\mathbf{x})} \right] \\
&= \mathbb{E}_{t \in [0,1], \mathbf{z} \sim q_t(\cdot|\mathbf{x})} \frac{\alpha'_t}{N\alpha_t} \left[-\frac{N}{\alpha_t N(\mathbf{x}_\theta)_i + (1 - \alpha_t)} + \frac{N}{\alpha_t N\mathbf{x}_i + (1 - \alpha_t)} \right. \\
&\quad \left. - \sum_{\mathbf{z}' \neq \mathbf{z}} \frac{q_t(\mathbf{z}'|\mathbf{x})}{q_t(\mathbf{z}|\mathbf{x})} \log \left(\frac{1}{\mathbf{s}_\theta(\mathbf{z})_{\mathbf{z}'}} \frac{q_t(\mathbf{z}'|\mathbf{x})}{q_t(\mathbf{z}|\mathbf{x})} \right) \right]
\end{aligned}$$

Using (43) and (44) we get,

$$\begin{aligned}
&= \mathbb{E}_{t \in [0,1], \mathbf{z} \sim q_t(\cdot|\mathbf{x})} \frac{\alpha'_t}{N\alpha_t} \left[\frac{N}{\alpha_t N\mathbf{x}_i + (1 - \alpha_t)} - \frac{N}{\alpha_t N(\mathbf{x}_\theta)_i + (1 - \alpha_t)} \right. \\
&\quad \left. - \sum_{\mathbf{z}' \neq \mathbf{z}} \frac{\alpha_t N\mathbf{x}_j + (1 - \alpha_t)}{\alpha_t N\mathbf{x}_i + (1 - \alpha_t)} \log \left(\frac{\alpha_t N(\mathbf{x}_\theta)_i + (1 - \alpha_t)}{\alpha_t N(\mathbf{x}_\theta)_j + (1 - \alpha_t)} \cdot \frac{\alpha_t N\mathbf{x}_j + (1 - \alpha_t)}{\alpha_t N\mathbf{x}_i + (1 - \alpha_t)} \right) \right] \\
&= \text{NELBO}_{\text{UDLM}}
\end{aligned}$$

C EXPERIMENTAL DETAILS

C.1 DATASET DETAILS

In this section, we provide more details, e.g., source, train/validation splits, etc., for the the datasets used in this work. For an overview, please see Table 8.

Species-10 This dataset is a composite of reference genomes from ten diverse species: *Arabidopsis thaliana*, *Caenorhabditis elegans*, *Danio rerio*, *Drosophila melanogaster*, *Felis catus*, *Gallus gallus*, *Gorilla gorilla*, *Homo sapiens*, *Mus musculus*, and *Salmo trutta*, which were downloaded from NCBI refseq database (O’Leary et al., 2016). In Table 9, we provide the assembly accession IDs used to download the reference genomes. Genomes were chunked into non-overlapping segments of 32,768 nucleotides and were tokenized using base-pair-level tokenization.

Training and validation sets were randomly split using 95% / 5%. In Table 10, we specify the size and relative species composition of each split.

Table 8: Relevant details for datasets used in this work.

Dataset	Tokenizer	Vocab. Size	Input size	Padding?
Species-10	Base-pair	12	32,768	No
QM9	Regex (Schwaller et al., 2019)	40	32	Yes
CIFAR-10	Binned Pixel Intensity	256	32×32×3	No
text8	Character	35	256	No
Amazon	bert-base-uncased	30,522	128	Yes
LM1B	bert-base-uncased	30,522	128	Yes

Table 9: Species genomes accession IDs

Species	Assembly Accession
<i>Arabidopsis thaliana</i>	GCF_000001735.4_TAIR10.1
<i>Caenorhabditis elegans</i>	GCF_000002985.6_WBcel235
<i>Danio rerio</i>	GCF_000002035.6_GRCz11
<i>Drosophila melanogaster</i>	GCF_000001215.4_Release_6_plus_ISO1_MT
<i>Felis catus</i>	GCF_018350175.1_F.catus_Fca126_mat1.0
<i>Gallus gallus</i>	GCF_016699485.2_bGalGal1.mat_broiler.GRCg7b
<i>Gorilla gorilla</i>	GCF_029281585.2_NHGRI_mGorGor1-v2.0_pri
<i>Homo sapiens</i>	GCF_000001405.40_GRCh38.p14
<i>Mus musculus</i>	GCF_000001635.27_GRCm39
<i>Salmo trutta</i>	GCF_901001165.1_fSalTru1.1

For guidance, we use the species label.

QM9 Molecules The QM9 dataset comes from Ruddigkeit et al. (2012) and Ramakrishnan et al. (2014). The dataset is comprised of ~133k small molecules. We process the dataset using the RDKit library (Landrum et al., 2013) to extract ‘canonical’ SMILES string representations and add the annotations for drug-likeness (QED) and ring-counts. The data are tokenized using a regular expression from Schwaller et al. (2019). Input lengths of 32 tokens were used for pre-training and generation experiments.

Training and validation sets were randomly split using 95% / 5%.

For guidance, we use a cutoff of 90th percentile for QED / ring count to generate binary labels.

CIFAR-10 This widely-used image dataset contains RGB images with 32 × 32 pixels. We use the provided train and test splits of 50,000 training images and 10,000 validation images. The dataset

Table 10: Species-10 train and validation splits statistics. Proportion of each species in the training and validation sets. Overall split size is indicated in parentheses in the column header.

Species	Train (95% ≈ 16.5B bps)	Validation (5% ≈ 869M bps)
<i>Arabidopsis thaliana</i>	0.68	0.77
<i>Caenorhabditis elegans</i>	0.58	0.58
<i>Danio rerio</i>	9.50	9.29
<i>Drosophila melanogaster</i>	0.08	0.73
<i>Felis catus</i>	13.94	14.05
<i>Gallus gallus</i>	6.04	5.93
<i>Gorilla gorilla</i>	20.40	20.19
<i>Homo sapiens</i>	18.89	19.22
<i>Mus musculus</i>	15.69	15.60
<i>Salmo trutta</i>	13.49	13.64

contains 10 classes of roughly equal proportion. We tokenize the dataset by rounding to integer pixel intensity values in the range $[0, 255]$.

For guidance, we use the image class label.

text8 The dataset was downloaded from <http://matmahoney.net/dc/text8.zip>. Data was tokenized at the character level using the lower case letters [`'a'` - `'z'`] and a white-space character. The data was broken into non-overlapping chunks of 256 tokens.

The first 90M characters were used for the training set and the final 5M characters were used as a validation set.

Amazon Review The Amazon Review dataset was downloaded from https://huggingface.co/datasets/fancyzhx/amazon_polarity. We tokenize using the `bert-base-uncased` tokenizer. Sequences were padded to a max input length of 128 tokens.

Train and validation splits were used from the downloaded data, with 3.6 M sequences in the training data and 400k sequences in the validation set.

LM1B This dataset was downloaded from <https://huggingface.co/datasets/billion-word-benchmark/lm1b>. We tokenize using the `bert-base-uncased` tokenizer. Sequences were padded to a max input length of 128 tokens.

We use the train and validation splits provided in the downloaded data. After chunking the data, our training set consisted of 7M sequences and our validation set consisted of 72k sequences.

C.2 ARCHITECTURAL DETAILS

In Table 11, we provide an overview of the architectures and parameter counts of the models used for each dataset.

Table 11: Architectures used when training on various datasets.

Dataset	Architecture	Parameter Count
Species-10	Mamba (AR) / Caduceus (Diffusion)	3.5 M (AR) / 4.8 M (Diffusion)
QM9	Transformer	92.4 M
CIFAR-10	UNet	35.8 M
Text8	Transformer	92.4 M
Amazon	Transformer	139 M
LM1B	Transformer	139 M

Genomics Caduceus For the Species-10 experiments, we use Mamba-based models (Gu & Dao, 2023). The AR model is a standard next-token-prediction Mamba backbone with 8 blocks and hidden dimension 256. For the diffusion models we train with a variant of the Caduceus architecture from Schiff et al. (2024), also with 8 blocks and hidden dimension 256. Specifically, we use the non-reverse complementary equivariant version of Caduceus, dubbed Caduceus-Ph in Schiff et al. (2024), which is similar to the AR Mamba, but with bi-directional Mamba blocks that use strategic weight tying to limit the parameter count: 3.5 M parameters of AR vs. 4.8 M for diffusion models.

CIFAR-10 UNet We adopt the UNet (Ronneberger et al., 2015) as a main backbone for both MDLM and UDLM, following (Ho et al., 2020). Network configurations are presented in Table 12. Specifically, we follow Austin et al. (2021) and Campbell et al. (2022) and use the original UNet backbone from DDPM (Ho et al., 2020), adding an extra discretized truncated logistic transformation to network outputs. To enable conditioning on labels, we add a label embedding layer which is added to the time embeddings, inspired by ADM network (Dhariwal & Nichol, 2021b).

Table 12: Architecture details for CIFAR-10 UNet.

	MDLM	UDLM
Vocab size	258	256
Number of ResNet blocks per scale	2	2
Base channels	128	128
Channel multiplier per scale	(1,2,2,2)	(1,2,2,2)
Attention resolutions	16	16
Time conditioning	False	True
Conditional embedding dimension	128	128
Number of Params	35.8M	35.8M

QM9 and NLP Transformer For both the QM9 and NLP datasets (Amazon, text8, and LM1B), we use the same Diffusion Transformer (Peebles & Xie, 2023) with adaLN for conditioning on time (for uniform noise diffusion models) and class (for guided generation). The Transformer for each dataset differs only in the word-embedding size, which is determined by the vocabulary size of the datasets’ corresponding tokenizer. Our Transformer consists of 12 layers, a hidden dimension of 768, and 12 attention heads. We use RoPE (Su et al., 2021) as the positional embeddings.

C.3 TRAINING CONFIGURATIONS

In Table 13, we detail the hyperparameter setup for each of the language modeling experiments in Section 5.1.

All diffusion models were trained and evaluated using a log-linear noise schedule.

Of note, for CIFAR-10, our models are trained for 300K iterations as opposed to 1.5M iterations, as in D3PM (Austin et al., 2021).

Table 13: Training hyper-parameters for all included experiments.

	Species-10	QM9	CIFAR-10	text8	Amazon	LM1B
Train steps	30K	25K	300K	1000K	184K	1000K
Batch size	32	2048	512	512	512	512
LR	$2e^{-3}$	$3e^{-4}$	$2e^{-4}$	$3e^{-4}$	$3e^{-4}$	$3e^{-4}$
Optim.	ADAM (0.9, 0.999)	ADAM (0.9, 0.999)	ADAM (0.9, 0.999)	ADAM (0.9, 0.999)	ADAM (0.9, 0.999)	ADAM (0.9, 0.999)
LR sched.	CosineDecay $3e^{-6}$ min.	CosineDecay $3e^{-6}$ min.	-	-	-	-
Warmup steps	3K	1K	5K	2.5K	2.5K	2.5K
GPU count	8	4	8	8	8	8
GPU type	A5000	A6000	A100	A100	A5000	A100

C.4 GUIDANCE DETAILS

C.4.1 BASELINES

FUDGE Implementation FUDGE is a classifier-based autoregressive guidance method proposed by Yang & Klein (2021). FUDGE first trains a classifier on all possible prefixes. During sampling, instead of directly sampling from $p(x_i|x_{1:i-1})$, FUDGE samples from the perturbed conditional distribution $p(y|x_{1:i})p(x_i|x_{1:i-1})$ where y denotes the classifier label, $x_{1:i-1}$ denotes the already decoded tokens and x_i stands for possible token to be generated. For efficiency, FUDGE trun-

cates x_i to the $topk$ tokens with the largest unconditional log-likelihood. Although not in the original FUDGE formulation, following the classifier-based guidance in diffusion models (Dhariwal & Nichol (2021b)), we introduce the temperature variable γ and sample from the perturbed distribution

$$\frac{p(x_i|x_{1:i-1})p^\gamma(y|x_{1:i})}{\sum_{x_i} p(x_i|x_{1:i-1})p^\gamma(y|x_{1:i})}$$

In our QM9 experiments, $topk$ is set as the vocabulary size which is 40. When training the classifier, we use a smaller classification model using the same dataset specified in Appendix C.1. The smaller backbone DiT consists of 8 layers, 8 attention heads, and a hidden dimension of 512. We use the same hyperparameters as those specified in Table 13.

PPLM Implementation Inspired by the approximate Metropolis-adjusted Langevin (MALA), Plug and Play language model (PPLM Dathathri et al. (2019) introduces guidance by conducting gradient updates on the hidden representations of a language model. PPLM first rewrites the autoregressive language models’ decoding process using the KV-cache mechanism (Wolf et al., 2020): $x_{t+1}, H_{t+1} = LM(x_t, H_t)$, where x_t denotes the token at time step t and H_t is defined as $[(K_t^{(1)}, V_t^{(1)}), \dots, (K_t^{(l)}, V_t^{(l)})]$ in which l is the number of layers. When decoding the token x_{t+1} at time step $t + 1$, PPLM initializes the perturbation term ΔH_t as 0, and then iteratively updates it by n times following the gradient ascend formula: $\Delta H_t \leftarrow \Delta H_t + \eta \frac{\nabla_{\Delta H_t} [\log(p(y|H_t + \Delta H_t)) - \gamma_{KL} D_{KL}(p(x_{t+1}|H_t + \Delta H_t) || p(x_{t+1}|H_t))]}{\|\nabla_{\Delta H_t} [\log(p(y|H_t + \Delta H_t)) - \gamma_{KL} D_{KL}(p(x_{t+1}|H_t + \Delta H_t) || p(x_{t+1}|H_t))]\|}$ in which y denotes the classifier label. PPLM then generates the perturbed probability distribution $p_{perb}(x_{t+1}|H_t + \Delta H_t)$ using $H_t + \Delta H_t$ and decodes x_{t+1} using the fused probability distribution $\frac{1}{\beta} p_{perb}^{\gamma_{gm}}(x_{t+1}|H_t + \Delta H_t) p_{unperb}^{1-\gamma_{gm}}(x_{t+1}|H_t)$, where β is the normalization factor. Following Dathathri et al. (2019), in our experiments γ_{kl} is set as 0.01 and γ_{gm} is set as 0.95. η and n are decided by grid search.

For the QM9 experiments, when training the classifier for PPLM, we use the same dataset specified in Appendix C.1. We use the same hyperparameters as those specified in Table 13, except the LR peak is reduced to $3e^{-5}$ and minimum is reduced to $3e^{-7}$.

NOS Implementation To implement the NOS baseline from Gruver et al. (2024), we train a classifier where we use the same backbone as the unconditional diffusion model (see Appendix C.2 for architecture details), and we initialize and freeze weights using the pre-trained unconditional diffusion model. We then mean pool the last hidden embeddings of the backbone and linearly project them to the classification logits. This final projection layer represents the only trainable parameters of the guidance model.

At inference, we perform Langevin sampling following Algorithm 2 from Gruver et al. (2024). In our experiments we denote step-size for the Langevin sampling by η , the number of steps by n , and the weight on the ‘fluency’ KL penalty by γ_{kl} .

For the QM9 experiments, when training the classifier for NOS, we use the same dataset specified in Appendix C.1. We use the same hyperparameters as those specified in Table 13, except the LR peak is reduced to $3e^{-5}$ and minimum is reduced to $3e^{-7}$.

C.4.2 D-CFG DETAILS

When implementing D-CFG we train a single AR / discrete diffusion model (see Appendix C.2 for architecture details) where we randomly drop out the class condition by replacing it with a class [MASK] token. The class condition is fused into models using the implementation of adaptive layer norm from Peebles & Xie (2023). We use 10% rate for masking / dropping-out the condition.

At inference time, we perform two forward passes through the model, one with condition provided to compute the conditional probability $p_\theta(\mathbf{z}_s | \mathbf{z}_t, y)$ and one where the condition is masked to compute the unconditional probability $p_\theta(\mathbf{z}_s | \mathbf{z}_t)$. These values are then used as described in Section 3.1.

C.4.3 D-CBG DETAILS

For D-CBG in the QM9 experiment, we train a smaller classification model using the same dataset specified in Appendix C.1. The smaller backbone DiT consists of 8 layers, 8 attention heads, and a hidden dimension of 512. We apply mean pooling on the final hidden representations before

linearly projecting to the classification logits. We use the same hyperparameters as those specified in Table 13.

We train the model on noised inputs using a log-linear schedule, where the type of corruption applied corresponds to the diffusion model to which guidance is applied.

C.5 GUIDANCE EVALUATION DETAILS

C.5.1 GENOMIC SEQUENCES METRICS

Below we describe the quality and control metrics used in the species-specific genome generation experiment.

***k*-mer JS** To compute the *k*-mer distribution shift, for each species, we create counts for each of the unique 3mers and 6mers for that species in the validation set and 64 generated sequences for that species. We then compute the Jensen-Shannon divergence between those categorical histograms. Finally we take a weighted average of these distances across species where the weights are given by the relative species proportion in the validation dataset, see Table 10 for the relative proportions.

Discriminator AUROC For the discriminator AUROC metric, we train a HyenaDNA model with 2 layers and hidden dimension 128. This model was downloaded, modified (reduced number of layers and hidden dimension) and initialized from scratch from <https://huggingface.co/LongSafari/hyenaDNA-small-32k-seqlen-hf>. We mean pool the final layer embeddings and linearly project them to the binary classification logits. The model is trained on the 640 generated sequences, which are labeled as the negative class, and 640 randomly selected sequences from the ground truth validation set (64 sequences per species), which are labeled as the positive class. This dataset of 1,280 sequences is randomly split into 95% train and 5% validation. The discriminator is trained with batch size of 8, learning rate of $1e^{-4}$, and the ADAM optimizer for 3 epochs to minimize binary cross entropy loss on the classification of real vs. generated sequences. We report the AUROC from the final epoch on the 5% validation split of this classification dataset.

Oracle F1 Finally, controllability is measured by the macro-averaged F1 of an oracle model on the 640 generated sequences. Our oracle model is a separate HyenaDNA model with 8 layers and hidden dimension 256, which has 6.6M parameters. This model was downloaded and initialized from scratch from <https://huggingface.co/LongSafari/hyenaDNA-small-32k-seqlen-hf>. We mean pool the final layer embeddings and linearly project them to the ten category classification logits. This model was trained on the full Species-10 dataset as described in Appendix C.1. For reference, in Table 14 we present the classification results of the this oracle model in the 5% validation set of the original data. We see that other than difficulty distinguishing between human and gorilla genomes, the model can serve as a near perfect oracle.

Table 14: Evaluation of HyenaDNA ‘oracle’ classifier on Species10 validation split.

Species	Precision	Recall	F1
<i>Arabidopsis thaliana</i>	1.00	0.99	1.00
<i>Caenorhabditis elegans</i>	1.00	1.00	1.00
<i>Danio rerio</i>	1.00	1.00	1.00
<i>Drosophila melanogaster</i>	1.00	1.00	1.00
<i>Felis catus</i>	1.00	1.00	1.00
<i>Gallus gallus</i>	1.00	1.00	1.00
<i>Gorilla gorilla</i>	0.63	0.45	0.52
<i>Homo sapiens</i>	0.54	0.72	0.62
<i>Mus musculus</i>	1.00	0.97	0.98
<i>Salmo trutta</i>	1.00	0.98	0.99

1350 C.5.2 CIFAR-10 QUALITY METRICS

1351 For evaluation, we randomly samples 50,000 images for each model and the tools provided
 1352 here: [https://github.com/w86763777/pytorch-image-generation-metrics.](https://github.com/w86763777/pytorch-image-generation-metrics.git)
 1353 [git](https://github.com/w86763777/pytorch-image-generation-metrics.git), as described in Campbell et al. (2022).
 1354

1355 **FID** Fréchet inception distance (Heusel et al., 2017) is a common metric in image generation
 1356 where the divergence between real and generated data is measured to reflect the alignment of two
 1357 distributions. The metric uses features extracted from a pretrained Inception-v3 model on ImageNet-
 1358 1K to estimate the mean and variance of the input data. The difference of two multi-dimensional
 1359 Gaussian distributions is measured by Wasserstein-2 distance or Fréchet distance $d(\cdot)$ as follows:
 1360

$$1361 \text{FID} = d(\mathcal{N}(\mu_{real}, \Sigma_{real}), \mathcal{N}(\mu_{fake}, \Sigma_{fake})) = \|\mu_{real} - \mu_{fake}\| + \\ 1362 \|\text{Tr}(\Sigma_{real} + \Sigma_{fake} - 2(\Sigma_{real}\Sigma_{fake})^{0.5})\| \quad (47)$$

1363 **IS** Inception Score (Salimans et al., 2016) is an alternative measure of how well generated images
 1364 are aligned with human judgement. IS also utilizes Inception-v3 model to compute label distribution
 1365 $p(y|x)$ for each generated image. IS focuses on two criteria: (1) A generated image should contain a
 1366 distinct class object, meaning its label distribution is expected to have low entropy; (2) The generated
 1367 images should vary across multiple classes, so the marginal distribution, $p(y) = \int_z p(y|G(z))dz$, is
 1368 expected to have high entropy, ideally approaching a uniform distribution. The formula is presented
 1369 as below:
 1370

$$1371 IS = \exp [\mathbb{E}_x \text{KL}(p(y|x)||p(y))], \quad (48)$$

1372 **F1** F1 is used as a proxy for satisfying the desired conditional generation of gener-
 1373 ated samples by a pre-trained classifier on CIFAR-10. We use a pretrained Vision Trans-
 1374 former model downloaded from [https://huggingface.co/edadaltocg/vit_base_](https://huggingface.co/edadaltocg/vit_base_patch16_224_in21k_ft_cifar10)
 1375 [patch16_224_in21k_ft_cifar10](https://huggingface.co/edadaltocg/vit_base_patch16_224_in21k_ft_cifar10) and fine-tuned on CIFAR-10.
 1376

1377 C.5.3 QM9 GUIDANCE METRICS

1378 For the guidance experiments in QM9, we generate 2,048 sequences of length 32. The reported
 1379 metrics are explained below.

1380 **Validity** Validity is measured by whether the generated SMILES string can be parsed by the RDKit
 1381 library. Any strings that fail to be parsed are counted as invalid.

1382 **Novelty** Novelty is measured by the number of valid and unique sequences that are not present in
 1383 the original QM9 dataset.

1384 **Property Mean / Median** Finally, we also report the mean and median of the novel generated
 1385 sequence for the property of interest, QED or ring count.

1386 D GUIDANCE ABLATION RESULTS

1387 For each of the guidance experiments, we perform a hyperparameter search on the guidance param-
 1388 eters, e.g., γ in D-CFG and D-CBG. Below we present results from these searches for the various
 1389 guidance experiments.

1390 **Species-specific Genome Generation** In this experiment we vary $\gamma \in \{1, 2, 3\}$ for D-CFG ap-
 1391 plied to AR, MDLM, and UDLM. Additionally, for MDLM and UDLM we vary the number of
 1392 sampling steps $T \in \{128, 256, 512\}$.

1393 Results for the AR D-CFG grid search are presented in Table 15, results for MDLM and UDLM grid
 1394 search are presented in Table 16. These results highlight that UDLM is more amenable to guidance

Table 15: Varying γ for AR with D-CFG on Species-10 generation.

AR D-CFG γ	3-mer JS (\downarrow)	6-mer JS (\downarrow)	Disc. AUROC (\downarrow)	F1 (\uparrow)
1	0.04	0.09	1.00	0.87
2	0.05	0.14	1.00	0.68
3	0.10	0.23	1.00	0.20

Table 16: Varying γ and T for MDLM and UDLM with D-CFG on Species-10 generation.

Model	D-CFG γ	3-mer JS (\downarrow)	6-mer JS (\downarrow)	Disc. AUROC (\downarrow)	F1 (\uparrow)
$T = 128$					
MDLM	1	0.03	0.08	0.66	0.87
MDLM	2	0.04	0.12	0.89	0.77
MDLM	3	0.06	0.15	0.91	0.63
UDLM	1	0.03	0.08	0.72	0.91
UDLM	2	0.07	0.15	0.69	0.92
UDLM	3	0.10	0.23	0.74	0.83
$T = 256$					
MDLM	1	0.03	0.08	0.81	0.88
MDLM	2	0.04	0.11	0.84	0.77
MDLM	3	0.07	0.16	0.83	0.67
UDLM	1	0.03	0.09	0.84	0.95
UDLM	2	0.07	0.16	0.85	0.94
UDLM	3	0.11	0.24	0.93	0.81
$T = 512$					
MDLM	1	0.03	0.07	0.61	0.90
MDLM	2	0.04	0.11	0.71	0.78
MDLM	3	0.06	0.15	0.91	0.69
UDLM	1	0.03	0.08	0.77	0.92
UDLM	2	0.08	0.18	0.75	0.96
UDLM	3	0.11	0.24	0.76	0.82

than either AR or MDLM in this setting. UDLM achieves better quality and control metrics, and while all model performance degrades as $\gamma = 3$, UDLM degrades less and improves when $\gamma = 2$.

QM9 In this section, we list the hyperparameter grid search results for QM9 drug likeliness (QED) maximization using AR FUDGE (Table 17), AR PPLM (Table 18), AR CFG (Table 19), MDLM D-CBG (Table 20), MDLM D-CFG (Table 21), UDLM D-CBG (Table 22), UDLM D-CFG (Table 23), MDLM NOS (Table 24), and UDLM NOS (Table 25). QM9 ring count maximization guidance results with AR FUDGE (Table 26), AR PPLM (Table 27), AR D-CFG (Table 28), MDLM D-CBG (Table 29), MDLM D-CFG (Table 30), UDLM D-CBG (Table 31), UDLM D-CFG (Table 32), MDLM NOS (Table 33), UDLM NOS (Table 34) are also included.

CIFAR-10 In Table 35, we explore the effect of $\gamma \in 1, 2, 3, 4, 5$ in conditional image generation. We find that increasing γ generally leads to better IS and F1 scores for both MDLM and UDLM. For FID, MDLM achieves better scores as γ increases. However, the impact of γ is weaker for UDLM, as the model’s FID score worsens when γ exceeds 2. We also plot visual outputs of different γ in Figure 3. As γ is increased, the appearance and the shape of a class object become more refined and sharpened.

1458
 1459
 1460
 1461
 1462
 1463
 1464
 1465
 1466
 1467
 1468
 1469
 1470
 1471
 1472
 1473
 1474
 1475
 1476
 1477
 1478
 1479
 1480
 1481
 1482
 1483
 1484
 1485
 1486
 1487
 1488
 1489
 1490
 1491
 1492
 1493
 1494
 1495
 1496
 1497
 1498
 1499
 1500
 1501
 1502
 1503
 1504
 1505
 1506
 1507
 1508
 1509
 1510
 1511

Table 17: Varying γ for maximizing QED guidance with AR FUDGE. The number of generated molecules is 2048. Mean and median QED values of the novel molecules are reported. Best values are **bolded**. The set of results used in the main paper is starred.

γ	Num. Valid (\uparrow)	Num. Novel (\uparrow)	QED Mean (\uparrow)	QED Median (\uparrow)
1	2046	6	0.55	0.55
2	2034	18	0.56	0.56
3	1984	22	0.58	0.58
4	1833	31	0.56	0.57
5	1641	43	0.57	0.59
10*	914	24	0.58	0.60
15	674	10	0.58	0.60
20	434	7	0.57	0.59
25	200	5	0.62	0.62
30	77	4	0.62	0.62
35	18	7	0.61	0.61
40	9	4	0.61	0.61

Table 18: Varying η and n for maximizing QED guidance with AR PPLM. The number of generated molecules is 2048. Mean and median QED values of the novel molecules are reported. Best values are **bolded**. The set of results used in the main paper is starred.

	Num. Valid (\uparrow)	Num. Novel (\uparrow)	QED Mean (\uparrow)	QED Median (\uparrow)
$\eta = 0.04, n = 10$	2048	0	N.A.	N.A.
$\eta = 0.1, n = 10$	2044	22	0.43	0.46
$\eta = 0.04, n = 30$	2030	39	0.47	0.48
$\eta = 0.1, n = 30^*$	1618	291	0.48	0.49

Table 19: Varying γ for maximizing QED guidance with AR D-CFG. The number of generated molecules is 2048. Mean and median QED values of the novel molecules are reported. Best values are **bolded**. The set of results used in the main paper is starred.

γ	Num. Valid (\uparrow)	Num. Novel (\uparrow)	QED Mean (\uparrow)	QED Median (\uparrow)
1.0	2018	172	0.57	0.57
1.5	2018	175	0.58	0.58
2.0	2017	142	0.59	0.59
2.5*	1995	130	0.60	0.60
3.0	1954	121	0.60	0.60

1512
1513
1514
1515
1516
1517
1518
1519

Table 20: Varying γ for maximizing QED guidance with MDLM D-CBG. The number of generated molecules is 2048. Mean and median QED values of the novel molecules are reported. Best values are **bolded**. The set of results used in the main paper is starred.

γ	Num. Valid (\uparrow)	Num. Novel (\uparrow)	QED Mean (\uparrow)	QED Median (\uparrow)
1.0	1203	406	0.46	0.47
1.5	1061	369	0.47	0.47
2.0	902	310	0.48	0.48
2.5	801	271	0.48	0.49
3.0	711	216	0.49	0.50
3.5	629	189	0.50	0.52
4.0	542	173	0.50	0.51
4.5	489	154	0.51	0.53
5.0	423	135	0.52	0.53
5.5	402	123	0.53	0.54
6.0	362	115	0.53	0.55
6.5	338	110	0.54	0.56
7.0	343	95	0.55	0.56
7.5	292	88	0.55	0.56
8.0	276	73	0.56	0.58
8.5	294	72	0.56	0.56
9.0	267	73	0.56	0.57
9.5	270	71	0.56	0.58
10.0	248	69	0.56	0.57
15.0	151	54	0.57	0.58
20.0*	64	22	0.58	0.60
25.0	11	3	0.58	0.58
30.0	1	1	0.58	0.58
40.0	0	0	N.A.	N.A.

1544
1545
1546
1547
1548
1549
1550
1551

Table 21: Varying γ for maximizing QED guidance with MDLM D-CFG. The number of generated molecules is 2048. Mean and median QED values of the novel molecules are reported. Best values are **bolded**. The set of results used in the main paper is starred.

γ	Num. Valid (\uparrow)	Num. Novel (\uparrow)	QED Mean (\uparrow)	QED Median (\uparrow)
1.0	1178	410	0.56	0.57
1.5	1079	396	0.58	0.58
2.0	932	347	0.59	0.60
2.5	760	307	0.60	0.61
3.0*	652	251	0.61	0.61

1562
1563
1564
1565

1566

1567

1568

1569

1570

1571

Table 22: Varying γ for maximizing QED guidance with UDLM D-CBG. The number of generated molecules is 2048. Mean and median QED values of the novel molecules are reported. Best values are **bolded**. The set of results used in the main paper is starred.

1572

1573

1574

1575

1576

1577

1578

1579

1580

1581

1582

1583

1584

1585

1586

1587

1588

1589

Table 23: Varying γ for maximizing QED guidance with UDLM D-CFG. The number of generated molecules is 2048. Mean and median QED values of the novel molecules are reported. Best values are **bolded**. The set of results used in the main paper is starred.

1590

1591

1592

1593

1594

1595

1596

1597

1598

1599

1600

1601

1602

1603

1604

1605

1606

1607

1608

1609

1610

1611

1612

1613

1614

1615

1616

1617

1618

1619

γ	Num. Valid (\uparrow)	Num. Novel (\uparrow)	QED Mean (\uparrow)	QED Median (\uparrow)
1.0	2039	168	0.47	0.47
3.0	1916	154	0.50	0.50
5.0	1697	126	0.52	0.55
10.0	1771	63	0.57	0.59
15.0	1732	70	0.59	0.60
20.0	1670	77	0.60	0.60
25.0	1478	74	0.60	0.61
30.0	1330	69	0.60	0.61
35.0*	1223	87	0.61	0.61
40.0	1178	75	0.61	0.61

γ	Num. Valid (\uparrow)	Num. Novel (\uparrow)	QED Mean (\uparrow)	QED Median (\uparrow)
1.0	2010	184	0.57	0.57
1.5	2021	158	0.59	0.59
2.0	2032	144	0.60	0.60
2.5	2035	140	0.60	0.60
3.0*	2034	133	0.61	0.61



Figure 3: Illustration of varying γ on CIFAR-10.

1620
 1621
 1622
 1623
 1624
 1625
 1626
 1627
 1628
 1629
 1630
 1631
 1632
 1633
 1634
 1635
 1636
 1637
 1638
 1639
 1640
 1641
 1642
 1643
 1644
 1645
 1646
 1647
 1648
 1649
 1650
 1651
 1652
 1653
 1654
 1655
 1656
 1657
 1658
 1659
 1660
 1661
 1662
 1663
 1664
 1665
 1666
 1667
 1668
 1669
 1670
 1671
 1672
 1673

Table 24: Varying η , n , and γ_{kl} for maximizing QED guidance with MDLM NOS. The number of generated molecules is 2048. Mean and median QED values of the novel molecules are reported. Best values are **bolded**. The set of results used in the main paper is starred.

	Num. Valid (\uparrow)	Num. Novel (\uparrow)	QED (\uparrow)	
			Mean	Median
$\eta = 0.001, n = 1, \gamma_{kl} = 0$	1324	453	0.446	0.457
$\eta = 0.001, n = 1, \gamma_{kl} = 0.001$	1302	471	0.454	0.463
$\eta = 0.001, n = 1, \gamma_{kl} = 0.01^*$	1302	471	0.454	0.463
$\eta = 0.001, n = 5, \gamma_{kl} = 0$	1322	453	0.445	0.456
$\eta = 0.001, n = 5, \gamma_{kl} = 0.001$	1300	468	0.453	0.463
$\eta = 0.001, n = 5, \gamma_{kl} = 0.01$	1322	453	0.445	0.456
$\eta = 0.001, n = 10, \gamma_{kl} = 0$	1324	454	0.445	0.456
$\eta = 0.001, n = 10, \gamma_{kl} = 0.001$	1300	468	0.453	0.463
$\eta = 0.001, n = 10, \gamma_{kl} = 0.01$	1324	454	0.445	0.456
$\eta = 0.01, n = 1, \gamma_{kl} = 0$	1323	452	0.445	0.456
$\eta = 0.01, n = 1, \gamma_{kl} = 0.001$	1301	471	0.452	0.463
$\eta = 0.01, n = 1, \gamma_{kl} = 0.01$	1323	452	0.445	0.456
$\eta = 0.01, n = 5, \gamma_{kl} = 0$	1302	471	0.453	0.463
$\eta = 0.01, n = 5, \gamma_{kl} = 0.001$	1325	458	0.445	0.456
$\eta = 0.01, n = 5, \gamma_{kl} = 0.01$	1302	471	0.453	0.463
$\eta = 0.01, n = 10, \gamma_{kl} = 0$	1329	457	0.445	0.456
$\eta = 0.01, n = 10, \gamma_{kl} = 0.001$	1306	478	0.453	0.463
$\eta = 0.01, n = 10, \gamma_{kl} = 0.01$	1329	457	0.445	0.456
$\eta = 0.1, n = 1, \gamma_{kl} = 0$	1296	477	0.451	0.462
$\eta = 0.1, n = 1, \gamma_{kl} = 0.001$	1325	456	0.444	0.456
$\eta = 0.1, n = 1, \gamma_{kl} = 0.01$	1296	477	0.451	0.462
$\eta = 0.1, n = 5, \gamma_{kl} = 0$	1322	454	0.443	0.456
$\eta = 0.1, n = 5, \gamma_{kl} = 0.001$	1300	482	0.450	0.461
$\eta = 0.1, n = 5, \gamma_{kl} = 0.01$	1322	454	0.443	0.456
$\eta = 0.1, n = 10, \gamma_{kl} = 0$	1298	478	0.450	0.461
$\eta = 0.1, n = 10, \gamma_{kl} = 0.001$	1323	452	0.443	0.456
$\eta = 0.1, n = 10, \gamma_{kl} = 0.01$	1298	478	0.450	0.461
$\eta = 1, n = 1, \gamma_{kl} = 0$	1268	486	0.441	0.448
$\eta = 1, n = 1, \gamma_{kl} = 0.001$	1258	503	0.446	0.452
$\eta = 1, n = 1, \gamma_{kl} = 0.01$	1268	486	0.441	0.448
$\eta = 1, n = 5, \gamma_{kl} = 0$	1268	486	0.441	0.448
$\eta = 1, n = 5, \gamma_{kl} = 0.001$	1258	503	0.446	0.452
$\eta = 1, n = 5, \gamma_{kl} = 0.01$	1268	486	0.441	0.448
$\eta = 1, n = 10, \gamma_{kl} = 0$	1268	486	0.441	0.448
$\eta = 1, n = 10, \gamma_{kl} = 0.001$	1258	503	0.446	0.452
$\eta = 1, n = 10, \gamma_{kl} = 0.01$	1268	486	0.441	0.448
$\eta = 5, n = 1, \gamma_{kl} = 0$	631	367	0.435	0.443
$\eta = 5, n = 1, \gamma_{kl} = 0.001$	664	410	0.430	0.438
$\eta = 5, n = 1, \gamma_{kl} = 0.01$	631	367	0.435	0.443
$\eta = 5, n = 5, \gamma_{kl} = 0$	631	367	0.435	0.443
$\eta = 5, n = 5, \gamma_{kl} = 0.001$	664	410	0.430	0.438
$\eta = 5, n = 5, \gamma_{kl} = 0.01$	631	367	0.435	0.443
$\eta = 5, n = 10, \gamma_{kl} = 0$	631	367	0.435	0.443
$\eta = 5, n = 10, \gamma_{kl} = 0.001$	664	410	0.430	0.438
$\eta = 5, n = 10, \gamma_{kl} = 0.01$	631	367	0.435	0.443

1674
1675
1676
1677
1678
1679
1680
1681
1682
1683
1684
1685
1686
1687
1688
1689
1690
1691
1692
1693
1694
1695
1696
1697
1698
1699
1700
1701
1702
1703
1704
1705
1706
1707
1708
1709
1710
1711
1712
1713
1714
1715
1716
1717
1718
1719
1720
1721
1722
1723
1724
1725
1726
1727

Table 25: Varying η , n , and γ_{kl} for maximizing QED guidance with UDLM NOS. The number of generated molecules is 2048. Mean and median QED values of the novel molecules are reported. Best values are **bolded**. The set of results used in the main paper is starred.

	Num. Valid (\uparrow)	Num. Novel (\uparrow)	QED (\uparrow)	
			Mean	Median
$\eta = 0.001, n = 1, \gamma_{kl} = 0$	1976	369	0.450	0.462
$\eta = 0.001, n = 1, \gamma_{kl} = 0.001$	1988	383	0.458	0.467
$\eta = 0.001, n = 1, \gamma_{kl} = 0.01$	1988	383	0.458	0.467
$\eta = 0.001, n = 5, \gamma_{kl} = 0$	1987	382	0.458	0.467
$\eta = 0.001, n = 5, \gamma_{kl} = 0.001$	1975	369	0.449	0.462
$\eta = 0.001, n = 5, \gamma_{kl} = 0.01$	1987	382	0.458	0.467
$\eta = 0.001, n = 10, \gamma_{kl} = 0$	1987	379	0.457	0.467
$\eta = 0.001, n = 10, \gamma_{kl} = 0.001$	1976	369	0.449	0.462
$\eta = 0.001, n = 10, \gamma_{kl} = 0.01$	1987	379	0.457	0.467
$\eta = 0.01, n = 1, \gamma_{kl} = 0$	1988	384	0.458	0.467
$\eta = 0.01, n = 1, \gamma_{kl} = 0.001$	1976	373	0.450	0.462
$\eta = 0.01, n = 1, \gamma_{kl} = 0.01$	1988	384	0.458	0.467
$\eta = 0.01, n = 5, \gamma_{kl} = 0$	1976	370	0.449	0.461
$\eta = 0.01, n = 5, \gamma_{kl} = 0.001$	1985	383	0.458	0.468
$\eta = 0.01, n = 5, \gamma_{kl} = 0.01$	1985	383	0.458	0.468
$\eta = 0.01, n = 10, \gamma_{kl} = 0$	1974	371	0.449	0.461
$\eta = 0.01, n = 10, \gamma_{kl} = 0.001$	1988	383	0.458	0.468
$\eta = 0.01, n = 10, \gamma_{kl} = 0.01$	1974	371	0.449	0.461
$\eta = 0.1, n = 1, \gamma_{kl} = 0$	1976	384	0.448	0.461
$\eta = 0.1, n = 1, \gamma_{kl} = 0.001$	1985	387	0.458	0.468
$\eta = 0.1, n = 1, \gamma_{kl} = 0.01$	1976	384	0.448	0.461
$\eta = 0.1, n = 5, \gamma_{kl} = 0$	1984	380	0.459	0.468
$\eta = 0.1, n = 5, \gamma_{kl} = 0.001$	1973	377	0.449	0.462
$\eta = 0.1, n = 5, \gamma_{kl} = 0.01$	1984	380	0.459	0.468
$\eta = 0.1, n = 10, \gamma_{kl} = 0$	1982	382	0.459	0.468
$\eta = 0.1, n = 10, \gamma_{kl} = 0.001$	1973	375	0.449	0.462
$\eta = 0.1, n = 10, \gamma_{kl} = 0.01$	1982	382	0.459	0.468
$\eta = 1, n = 1, \gamma_{kl} = 0$	1965	361	0.455	0.466
$\eta = 1, n = 1, \gamma_{kl} = 0.001$	1957	382	0.452	0.461
$\eta = 1, n = 1, \gamma_{kl} = 0.01$	1965	361	0.455	0.466
$\eta = 1, n = 5, \gamma_{kl} = 0$	1957	382	0.452	0.461
$\eta = 1, n = 5, \gamma_{kl} = 0.001$	1965	361	0.455	0.466
$\eta = 1, n = 5, \gamma_{kl} = 0.01$	1957	382	0.452	0.461
$\eta = 1, n = 10, \gamma_{kl} = 0$	1957	382	0.452	0.461
$\eta = 1, n = 10, \gamma_{kl} = 0.001$	1965	361	0.455	0.466
$\eta = 1, n = 10, \gamma_{kl} = 0.01$	1957	382	0.452	0.461
$\eta = 5, n = 1, \gamma_{kl} = 0$	944	302	0.467	0.474
$\eta = 5, n = 1, \gamma_{kl} = 0.001$	974	329	0.465	0.470
$\eta = 5, n = 1, \gamma_{kl} = 0.01$	944	302	0.467	0.474
$\eta = 5, n = 5, \gamma_{kl} = 0$	944	302	0.467	0.474
$\eta = 5, n = 5, \gamma_{kl} = 0.001^*$	946	302	0.467	0.474
$\eta = 5, n = 5, \gamma_{kl} = 0.01$	981	332	0.465	0.469
$\eta = 5, n = 10, \gamma_{kl} = 0$	974	329	0.465	0.470
$\eta = 5, n = 10, \gamma_{kl} = 0.001$	975	330	0.465	0.470
$\eta = 5, n = 10, \gamma_{kl} = 0.01$	982	330	0.465	0.470

Table 26: Varying γ for maximizing Ring Count guidance with AR FUDGE. The number of generated molecules is 2048. Mean and Median Ring Count values of the novel molecules are reported. Best values are **bolded**. The set of results used in the main paper is starred.

γ	Num. Valid (\uparrow)	Num. Novel (\uparrow)	Ring Count Mean (\uparrow)	Ring Count Median (\uparrow)
1	2040	20	3.90	4.00
2*	2035	15	4.20	4.00
3	2018	11	5.09	5.00
4	1982	7	4.71	5.00
5	1785	3	5.33	6.00
10	1	0	N.A.	N.A.
15	0	0	N.A.	N.A.
20	0	0	N.A.	N.A.
25	0	0	N.A.	N.A.
30	0	0	N.A.	N.A.
35	0	0	N.A.	N.A.
40	0	0	N.A.	N.A.

Table 27: Varying η and n for maximizing Ring Count guidance with AR PPLM. The number of generated molecules is 2048. Mean and Median Ring Count values of the novel molecules are reported. Best values are **bolded**. The set of results used in the main paper is starred.

	Num. Valid (\uparrow)	Num. Novel (\uparrow)	Ring Count (\uparrow)	
			Mean	Median
$\eta = 0.04, n = 10$	2048	0	N.A.	N.A.
$\eta = 0.1, n = 10$	2042	23	1.26	1.00
$\eta = 0.04, n = 30$	2027	43	1.88	2.00
$\eta = 0.1, n = 30^*$	1486	233	1.89	2.00

Table 28: Varying γ for maximizing Ring Count guidance with AR D-CFG. The number of generated molecules is 2048. Mean and Median Ring Count values of the novel molecules are reported. Best values are **bolded**. The set of results used in the main paper is starred.

γ	Num. Valid (\uparrow)	Num. Novel (\uparrow)	Ring Count Mean (\uparrow)	Ring Count Median (\uparrow)
1.0	2009	303	4.49	4.00
1.5	1984	311	4.79	5.00
2.0	1948	390	4.77	5.00
2.5	1868	389	4.78	5.00
3.0	1765	378	4.82	5.00
3.5	1540	300	4.82	5.00
4.0	1206	217	4.88	5.00
4.5	965	173	4.71	4.00
5.0	656	110	4.75	4.00
5.5	426	76	4.70	4.00
6.0	284	57	4.75	4.00
6.5	166	35	4.92	5.00
7.0*	108	24	5.04	5.50
7.5	72	12	5.23	6.00
8.0	50	6	5.33	6.00
8.5	22	3	5.50	6.00
9.0	8	4	5.50	6.00
9.5	4	3	5.33	6.00
10.0	2	1	6.00	6.00

1782 Table 29: Varying γ for maximizing Ring Count guidance with MDLM D-CBG. The number of
 1783 generated molecules is 2048. Mean and Median Ring Count values of the novel molecules are
 1784 reported. Best values are **bolded**. The set of results used in the main paper is starred.

γ	Num. Valid (\uparrow)	Num. Novel (\uparrow)	Ring Count Mean (\uparrow)	Ring Count Median (\uparrow)
1.0	1160	447	2.19	2.00
5.0	364	215	3.58	4.00
10.0	251	160	4.19	4.00
15.0	171	118	4.71	5.00
20.0	119	100	4.98	5.00
25.0*	82	65	5.05	5.00
30.0	49	38	4.63	4.00
35.0	21	18	4.89	5.00
40.0	12	12	4.75	5.00

1796 Table 30: Varying γ for maximizing Ring Count guidance with MDLM D-CFG. The number of
 1797 generated molecules is 2048. Mean and Median Ring Count values of the novel molecules are
 1798 reported. Best values are **bolded**. The set of results used in the main paper is starred.

γ	Num. Valid (\uparrow)	Num. Novel (\uparrow)	Ring Count Mean (\uparrow)	Ring Count Median (\uparrow)
1.0	968	487	4.32	4.00
1.5	870	432	4.64	4.00
2.0	781	429	4.72	5.00
2.5	637	375	4.87	5.00
3.0	508	290	4.84	5.00
3.5	435	256	4.79	5.00
4.0	336	196	4.92	5.00
4.5	308	186	4.83	5.00
5.0	213	123	4.86	5.00
5.5	164	107	4.86	5.00
6.0*	132	90	5.01	5.00
6.5	81	54	4.80	5.00
7.0	77	54	4.83	5.00
7.5	54	39	4.82	5.00
8.0	32	22	4.68	5.00
8.5	17	14	4.64	4.00
9.0	10	9	4.78	5.00
9.5	12	11	4.91	5.00
10.0	3	3	4.00	4.00

1821 Table 31: Varying γ for maximizing Ring Count guidance with UDLM D-CBG. The number of
 1822 generated molecules is 2048. Mean and Median Ring Count values of the novel molecules are
 1823 reported. Best values are **bolded**. The set of results used in the main paper is starred.

γ	Num. Valid (\uparrow)	Num. Novel (\uparrow)	Ring Count Mean (\uparrow)	Ring Count Median (\uparrow)
1.0	2029	209	2.13	2.00
5.0	1494	301	4.09	4.00
10.0	1641	528	4.50	4.00
15.0	1676	711	4.56	4.00
20.0	1692	821	4.62	4.00
25.0	1697	849	4.66	4.00
30.0	1697	889	4.67	4.00
35.0	1707	926	4.71	4.00
40.0*	1670	943	4.73	5.00

1836
1837
1838
1839
1840
1841
1842
1843
1844
1845
1846
1847
1848
1849
1850
1851
1852
1853
1854
1855
1856
1857
1858
1859
1860
1861
1862
1863
1864
1865
1866
1867
1868
1869
1870
1871
1872
1873
1874
1875
1876
1877
1878
1879
1880
1881
1882
1883
1884
1885
1886
1887
1888
1889

Table 32: Varying γ for maximizing Ring Count guidance with UDLM D-CFG. The number of generated molecules is 2048. Mean and Median Ring Count values of the novel molecules are reported. Best values are **bolded**. The set of results used in the main paper is starred.

γ	Num. Valid (\uparrow)	Num. Novel (\uparrow)	Ring Count Mean (\uparrow)	Ring Count Median (\uparrow)
1.0	1932	585	4.54	4.00
1.5	1979	552	4.66	4.00
2.0	1981	535	4.80	5.00
2.5	1971	507	4.83	5.00
3.0	1968	481	4.82	5.00
3.5*	1975	459	4.91	5.00
4.0	1951	426	4.89	5.00
4.5	1925	404	4.88	5.00
5.0	1894	429	4.81	5.00
5.5	1826	406	4.89	5.00
6.0	1699	366	4.84	5.00
6.5	1611	317	4.83	5.00
7.0	1508	300	4.82	5.00
7.5	1375	308	4.84	5.00
8.0	1251	232	4.85	5.00
8.5	1110	219	4.81	5.00
9.0	1026	233	4.73	5.00
9.5	887	194	4.84	5.00
10.0	829	207	4.71	4.00

1890
 1891
 1892
 1893
 1894
 1895
 1896
 1897
 1898
 1899
 1900
 1901
 1902
 1903
 1904
 1905
 1906
 1907
 1908
 1909
 1910
 1911
 1912
 1913
 1914
 1915
 1916
 1917
 1918
 1919
 1920
 1921
 1922
 1923
 1924
 1925
 1926
 1927
 1928
 1929
 1930
 1931
 1932
 1933
 1934
 1935
 1936
 1937
 1938
 1939
 1940
 1941
 1942
 1943

Table 33: Varying η , n , and γ_{kl} for maximizing Ring Count guidance with MDLM NOS. The number of generated molecules is 2048. Mean and median Ring Count values of the novel molecules are reported. Best values are **bolded**. The set of results used in the main paper is starred.

	Num. Valid (\uparrow)	Num. Novel (\uparrow)	Ring Count (\uparrow)	
			Mean	Median
$\eta = 0.001, n = 1, \gamma_{kl} = 0$	1302	471	1.926	2.000
$\eta = 0.001, n = 1, \gamma_{kl} = 0.001$	1325	453	1.899	2.000
$\eta = 0.001, n = 1, \gamma_{kl} = 0.01$	1302	471	1.926	2.000
$\eta = 0.001, n = 5, \gamma_{kl} = 0$	1326	456	1.908	2.000
$\eta = 0.001, n = 5, \gamma_{kl} = 0.001$	1303	473	1.930	2.000
$\eta = 0.001, n = 5, \gamma_{kl} = 0.01$	1326	456	1.908	2.000
$\eta = 0.001, n = 10, \gamma_{kl} = 0$	1325	456	1.914	2.000
$\eta = 0.001, n = 10, \gamma_{kl} = 0.001$	1303	471	1.930	2.000
$\eta = 0.001, n = 10, \gamma_{kl} = 0.01$	1325	456	1.914	2.000
$\eta = 0.01, n = 1, \gamma_{kl} = 0$	1324	453	1.925	2.000
$\eta = 0.01, n = 1, \gamma_{kl} = 0.001$	1306	472	1.928	2.000
$\eta = 0.01, n = 1, \gamma_{kl} = 0.01$	1324	453	1.925	2.000
$\eta = 0.01, n = 5, \gamma_{kl} = 0$	1302	469	1.928	2.000
$\eta = 0.01, n = 5, \gamma_{kl} = 0.001$	1323	459	1.939	2.000
$\eta = 0.01, n = 5, \gamma_{kl} = 0.01$	1302	469	1.928	2.000
$\eta = 0.01, n = 10, \gamma_{kl} = 0$	1324	460	1.933	2.000
$\eta = 0.01, n = 10, \gamma_{kl} = 0.001$	1324	460	1.933	2.000
$\eta = 0.01, n = 10, \gamma_{kl} = 0.01$	1305	470	1.932	2.000
$\eta = 0.1, n = 1, \gamma_{kl} = 0$	1292	478	1.948	2.000
$\eta = 0.1, n = 1, \gamma_{kl} = 0.001$	1320	469	1.942	2.000
$\eta = 0.1, n = 1, \gamma_{kl} = 0.01$	1292	478	1.948	2.000
$\eta = 0.1, n = 5, \gamma_{kl} = 0$	1316	474	1.951	2.000
$\eta = 0.1, n = 5, \gamma_{kl} = 0.001$	1291	480	1.960	2.000
$\eta = 0.1, n = 5, \gamma_{kl} = 0.01$	1316	474	1.951	2.000
$\eta = 0.1, n = 10, \gamma_{kl} = 0$	1315	471	1.951	2.000
$\eta = 0.1, n = 10, \gamma_{kl} = 0.001$	1292	480	1.952	2.000
$\eta = 0.1, n = 10, \gamma_{kl} = 0.01$	1292	480	1.952	2.000
$\eta = 1, n = 1, \gamma_{kl} = 0$	1186	507	2.384	2.000
$\eta = 1, n = 1, \gamma_{kl} = 0.001$	1163	479	2.240	2.000
$\eta = 1, n = 1, \gamma_{kl} = 0.01$	1186	507	2.384	2.000
$\eta = 1, n = 5, \gamma_{kl} = 0$	1186	507	2.384	2.000
$\eta = 1, n = 5, \gamma_{kl} = 0.001$	1188	510	2.388	2.000
$\eta = 1, n = 5, \gamma_{kl} = 0.01$	1166	481	2.263	2.000
$\eta = 1, n = 10, \gamma_{kl} = 0$	1163	479	2.240	2.000
$\eta = 1, n = 10, \gamma_{kl} = 0.001$	1188	508	2.391	2.000
$\eta = 1, n = 10, \gamma_{kl} = 0.01$	1168	483	2.267	2.000
$\eta = 5, n = 1, \gamma_{kl} = 0$	390	268	3.164	3.000
$\eta = 5, n = 1, \gamma_{kl} = 0.001$	337	231	3.147	3.000
$\eta = 5, n = 1, \gamma_{kl} = 0.01$	390	268	3.164	3.000
$\eta = 5, n = 5, \gamma_{kl} = 0$	390	268	3.164	3.000
$\eta = 5, n = 5, \gamma_{kl} = 0.001$	341	235	3.187	3.000
$\eta = 5, n = 5, \gamma_{kl} = 0.01$	403	281	3.281	3.000
$\eta = 5, n = 10, \gamma_{kl} = 0$	390	268	3.164	3.000
$\eta = 5, n = 10, \gamma_{kl} = 0.001$	343	237	3.203	3.000
$\eta = 5, n = 10, \gamma_{kl} = 0.01^*$	353	246	3.313	3.000

Table 34: Varying η , n , and γ_{kl} for maximizing Ring Count guidance with UDLM NOS. The number of generated molecules is 2048. Mean and median Ring Count values of the novel molecules are reported. Best values are **bolded**. The set of results used in the main paper is starred.

		Num. Valid (\uparrow)	Num. Novel (\uparrow)	Ring Count (\uparrow)	
				Mean	Median
1944					
1945					
1946					
1947					
1948					
1949					
1950					
1951					
1952					
1953					
1954	$\eta = 0.001, n = 1, \gamma_{kl} = 0$	1975	369	2.024	2.000
1955	$\eta = 0.001, n = 1, \gamma_{kl} = 0.001$	1987	382	2.026	2.000
1956	$\eta = 0.001, n = 1, \gamma_{kl} = 0.01$	1987	382	2.026	2.000
1957	$\eta = 0.001, n = 5, \gamma_{kl} = 0$	1975	369	2.014	2.000
1958	$\eta = 0.001, n = 5, \gamma_{kl} = 0.001$	1987	379	2.021	2.000
1959	$\eta = 0.001, n = 5, \gamma_{kl} = 0.01$	1975	369	2.014	2.000
1960	$\eta = 0.001, n = 10, \gamma_{kl} = 0$	1987	382	2.016	2.000
1961	$\eta = 0.001, n = 10, \gamma_{kl} = 0.001$	1975	369	2.014	2.000
1962	$\eta = 0.001, n = 10, \gamma_{kl} = 0.01$	1975	369	2.014	2.000
1963	$\eta = 0.01, n = 1, \gamma_{kl} = 0$	1975	373	2.024	2.000
1964	$\eta = 0.01, n = 1, \gamma_{kl} = 0.001$	1987	376	2.027	2.000
1965	$\eta = 0.01, n = 1, \gamma_{kl} = 0.01$	1987	376	2.027	2.000
1966	$\eta = 0.01, n = 5, \gamma_{kl} = 0$	1973	373	2.019	2.000
1967	$\eta = 0.01, n = 5, \gamma_{kl} = 0.001$	1989	384	2.026	2.000
1968	$\eta = 0.01, n = 5, \gamma_{kl} = 0.01$	1989	384	2.026	2.000
1969	$\eta = 0.01, n = 10, \gamma_{kl} = 0$	1971	372	2.027	2.000
1970	$\eta = 0.01, n = 10, \gamma_{kl} = 0.001$	1990	384	2.034	2.000
1971	$\eta = 0.01, n = 10, \gamma_{kl} = 0.01$	1971	372	2.027	2.000
1972	$\eta = 0.1, n = 1, \gamma_{kl} = 0$	1983	387	2.041	2.000
1973	$\eta = 0.1, n = 1, \gamma_{kl} = 0.001$	1973	371	1.997	2.000
1974	$\eta = 0.1, n = 1, \gamma_{kl} = 0.01$	1983	387	2.041	2.000
1975	$\eta = 0.1, n = 5, \gamma_{kl} = 0$	1983	391	2.087	2.000
1976	$\eta = 0.1, n = 5, \gamma_{kl} = 0.001$	1974	367	1.989	2.000
1977	$\eta = 0.1, n = 5, \gamma_{kl} = 0.01$	1974	367	1.989	2.000
1978	$\eta = 0.1, n = 10, \gamma_{kl} = 0$	1981	392	2.094	2.000
1979	$\eta = 0.1, n = 10, \gamma_{kl} = 0.001$	1975	371	1.992	2.000
1980	$\eta = 0.1, n = 10, \gamma_{kl} = 0.01$	1981	392	2.094	2.000
1981	$\eta = 1, n = 1, \gamma_{kl} = 0$	1961	423	2.137	2.000
1982	$\eta = 1, n = 1, \gamma_{kl} = 0.001$	1962	403	2.181	2.000
1983	$\eta = 1, n = 1, \gamma_{kl} = 0.01$	1961	423	2.137	2.000
1984	$\eta = 1, n = 5, \gamma_{kl} = 0$	1961	423	2.137	2.000
1985	$\eta = 1, n = 5, \gamma_{kl} = 0.001$	1962	403	2.181	2.000
1986	$\eta = 1, n = 5, \gamma_{kl} = 0.01$	1961	423	2.137	2.000
1987	$\eta = 1, n = 10, \gamma_{kl} = 0$	1961	423	2.137	2.000
1988	$\eta = 1, n = 10, \gamma_{kl} = 0.001$	1962	403	2.181	2.000
1989	$\eta = 1, n = 10, \gamma_{kl} = 0.01$	1961	423	2.137	2.000
1990	$\eta = 5, n = 1, \gamma_{kl} = 0$	950	396	2.629	2.000
1991	$\eta = 5, n = 1, \gamma_{kl} = 0.001$	933	379	2.546	2.000
1992	$\eta = 5, n = 1, \gamma_{kl} = 0.01$	950	396	2.629	2.000
1993	$\eta = 5, n = 5, \gamma_{kl} = 0$	950	396	2.629	2.000
1994	$\eta = 5, n = 5, \gamma_{kl} = 0.001$	933	379	2.546	2.000
1995	$\eta = 5, n = 5, \gamma_{kl} = 0.01$	954	397	2.635	2.000
1996	$\eta = 5, n = 10, \gamma_{kl} = 0$	950	396	2.629	2.000
1997	$\eta = 5, n = 10, \gamma_{kl} = 0.001$	932	378	2.550	2.000
	$\eta = 5, n = 10, \gamma_{kl} = 0.01^*$	961	402	2.637	2.500

1998
1999
2000
2001
2002
2003
2004
2005
2006
2007
2008
2009
2010
2011
2012
2013
2014
2015
2016
2017
2018
2019
2020
2021
2022
2023
2024
2025
2026
2027
2028
2029
2030
2031
2032
2033
2034
2035
2036
2037
2038
2039
2040
2041
2042
2043
2044
2045
2046
2047
2048
2049
2050
2051

Table 35: Ablation results of γ values on CIFAR-10. Best values are **bolded**.

	FID (\downarrow)	IS (\uparrow)	F1 (\uparrow)
MDLM D-CFG			
$\gamma = 1$	27.94	7.14	0.76
$\gamma = 2$	18.62	8.24	0.95
$\gamma = 3$	16.19	8.78	0.99
$\gamma = 4$	15.56	9.02	0.99
$\gamma = 5$	15.73	9.19	1.00
UDLM D-CFG			
$\gamma = 1$	26.70	7.43	0.81
$\gamma = 2$	20.75	8.34	0.96
$\gamma = 3$	21.31	8.52	0.98
$\gamma = 4$	23.21	8.66	0.99
$\gamma = 5$	26.15	8.60	0.99